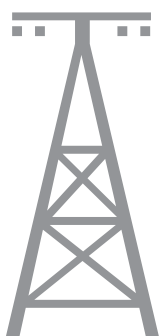
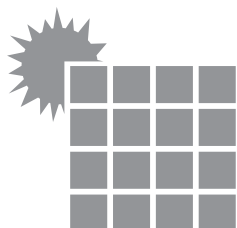


ISSN 2720-3581



# JOURNAL

OF GEOTECHNOLOGY  
AND ENERGY

FORMERLY AGH DRILLING, OIL, GAS

2021, vol. 38, no. 2

The “Journal of Geotechnology and Energy” (formerly “AGH Drilling, Oil, Gas”) is a quarterly published by the Faculty of Drilling, Oil and Gas at the AGH University of Science and Technology, Krakow, Poland. Journal is an interdisciplinary, international, peer-reviewed, and open access. The articles published in JGE have been given a favorable opinion by the reviewers designated by the editorial board.

## **Editorial Team**

### **Editor-in-chief**

Dariusz Knez, AGH University of Science and Technology, Poland

### **Co-editors**

Szymon Kuczyński  
Małgorzata Maria Formela  
Karol Dąbrowski  
Katarzyna Chruszcz-Lipska  
Rafał Matuła  
Sławomir Wysocki

### **Editorial Board**

Rafał Wiśniowski  
Danuta Bielewicz  
Stanisław Dubiel  
Andrzej Gonet  
Maciej Kaliski  
Stanisław Nagy  
Stanisław Rychlicki  
Jakub Siemek  
Jerzy Stopa  
Kazimierz Twardowski

### **Publisher**

AGH University of Science and Technology Press

Linguistic corrector: *Aeddan Shaw*

Technical editor: *Kamila Zimnicka*

Desktop publishing: *Munda*

Cover design: *Paweł Sepielak*

© Wydawnictwa AGH, Krakow 2021

Creative Commons CC-BY 4.0 License

ISSN: 2720-3581

DOI: <https://doi.org/10.7494/jge>

Journal website: <https://journals.agh.edu.pl/jge>

---

Wydawnictwa AGH (AGH University of Science and Technology Press)

al. A. Mickiewicza 30, 30-059 Kraków

tel. 12 617 32 28, 12 636 40 38

e-mail: [redakcja@wydawnictwoagh.pl](mailto:redakcja@wydawnictwoagh.pl)

<http://www.wydawnictwoagh.pl>

<http://www.wydawnictwo.agh.edu.pl>

---

# CONTENTS

---

Michał Maruta	
<b>The Potential Use of a Dräger X-am 8000 Portable Multi-gas Detector for Monitoring Explosive Gases in the Area of Historical Oil and Gas Fields in the Podkarpackie Region</b>	<b>5</b>
Magdalena Sowa-Zyzańska	
<b>Elements of Reservoir Simulation for Tight Gas Reservoirs with Water Influx</b>	<b>15</b>
Paweł Zyzański	
<b>Performance analysis of a horizontal well located in an underground gas storage facility</b>	<b>25</b>





Michał Maruta

ORCID: 0000-0002-1642-8189  
AGH University of Science and Technology in Krakow

## THE POTENTIAL USE OF A DRÄGER X-AM 8000 PORTABLE MULTI-GAS DETECTOR FOR MONITORING EXPLOSIVE GASES IN THE AREA OF HISTORICAL OIL AND GAS FIELDS IN THE PODKARPACIE REGION

Date of submission:  
23.06.2021

Date of acceptance:  
28.06.2021

Date of publication:  
31.08.2021

© 2021 Author. This is an open access publication, which can be used, distributed, and reproduced in any medium according to the Creative Commons CC-BY 4.0 License

<https://journals.agh.edu.pl/jge>

**Abstract:** The oldest oil basin in the world is located in the Polish Carpathians. Former mines, often abandoned, have become technical monuments. The growing popularity of industrial tourism in the world and in Poland attracts more and more tourists who want to “find oil” on their own. In most cases, these are abandoned crude oil and natural gas fields, with such places associated with the risk of poisoning, ignition or explosion of escaping gases from unprotected crude oil fields or borehole outlets. The article also highlights the heritage of oil mining in the Polish Carpathians and related cultural routes. The author focuses on the issue related to the occurrence of the hazard zone of hydrogen sulphide poisoning or methane explosion in the sites of old oil fields. It presents the possibility of using the Dräger X-am 8000 portable multi-gas detector as a personal device for monitoring the concentration of gases and vapours considered toxic and/or explosive, such as methane or hydrogen sulphide. It also proposes the use of the Dräger X-am 8000 multi-gas detector, which in combination with the Dräger X-site Live real-time area monitoring module, can serve as a mobile system for short- or long-term monitoring of the above-mentioned zones.

**Keywords:** Methane exhalation, hydrogen sulphide, hand-dug wells, industrial heritage tourism, Dräger X-am 8000

# 1. Introduction

Tourism is becoming a mass phenomenon, one which can almost be considered universal, and which is developing dynamically [1–3]. Furthermore, there is an increasing specialization of tourism, with technical monuments becoming tourist attractions. The division of tourism related to industry can be found in the work of M. Kronenberg [1], he distinguishes between:

- industrial tourism,
- tourism in post-industrial areas,
- industrial heritage tourism.

In reference to the rich heritage of the oil industry, new cultural routes are being created in the area of the Polish and Ukrainian Carpathians and existing ones are being modernized. They are located mainly in the Podkarpackie, Małopolska and Western Ukraine provinces [2, 4–9].

The most important of them include:

- The Jasło – Lviv Cross-Border Oil Trail,
- Carpathian-Galician Oil Trail,
- The World Cradle of Oil Mining,
- Following the footsteps of giant extinct mammals, earth wax, crude oil and salt.

It is worth remembering that contemporary responsible management of non-renewable energy sources requires reaching back to the 19th and 20th century history and the beginnings of oil and gas extraction.

The Carpathian oil and gas area is located in the central and eastern part of the Polish flysch Carpathians. The oil industry in Poland was initiated by hand-dug wells – known as dug pits, wells, and dug pits [10, 11]. Their location (Fig. 1) is the place of the primary, natural oil spill and/or exhalation of natural gas to the earth's surface.

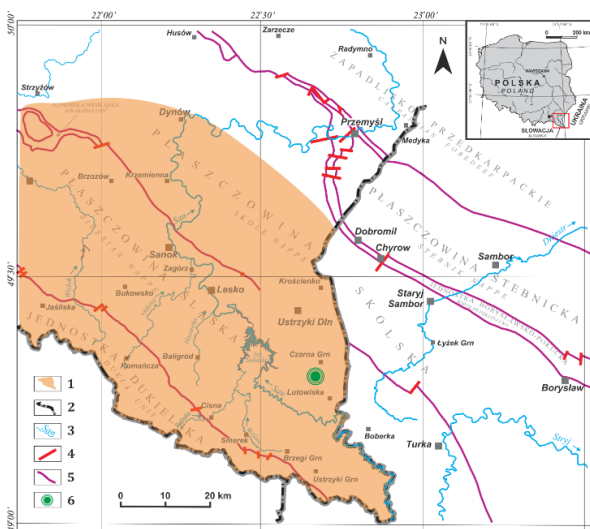


**Fig. 1.** The area of old hand-dug wells in the Polish Carpathians: 1 – range of the area of old mining pits occurrence, 2 – state borders; 3 – major rivers; 4 – faults; 5 – overthrusts, 6 – location of hand-dug well in Polana Ostre [12 – modified]

# 2. The risk associated with the exaltation of the gases in place of an old, abandoned oil and natural gas fields

Natural surface occurrence of oil and gas was known here already in the Middle Ages. The Polish geologist Stanisław Staszic, in his book *About Earthborn of the Carpathians and other mountains and Polish plains* [13] mentioned a black smudge of oil from the rocks [10, 14].

Old, abandoned oil and gas fields are becoming increasingly popular among tourists. Of these, the most interesting are the places where crude oil is available at one's fingertips and where the exhalations of natural gas are also visible (Fig. 2). Such places are often unmarked and unsecured [5–9, 15–18].

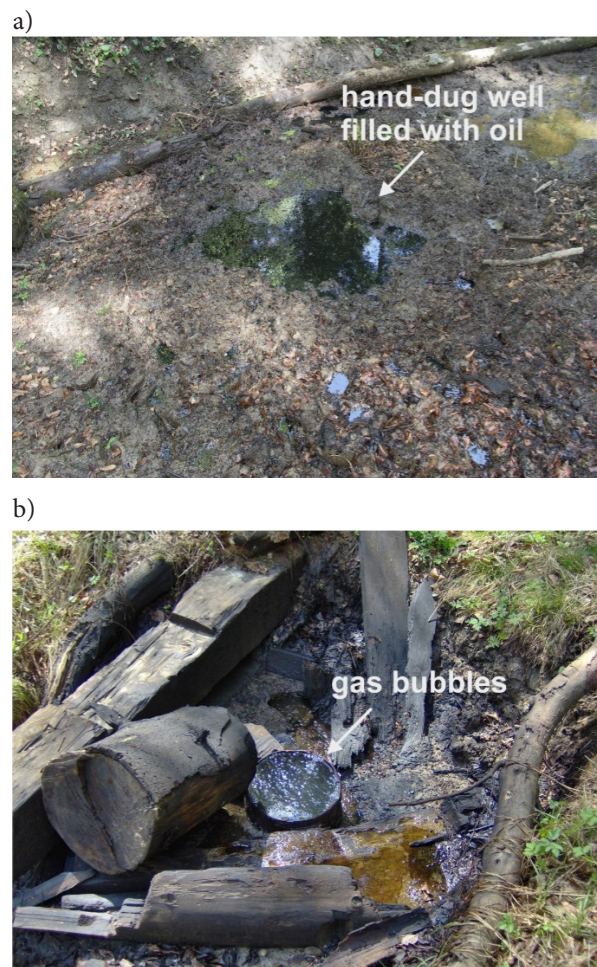


**Fig. 2.** An example of an old hand-dug set near Polana Ostre village: a) visible outline of the walls of the old hand-dug filled with oil; b) open outlet of the borehole with visible bubbles of methane [19 – modified]

Most often they have the form of hand-dug wooden wells or left-over boreholes (Fig. 3) [11, 19]. Oil was also obtained by collecting it from the water surface and digging shallow pits in the ground where it could accumulate.

According to the applications of the indigenous inhabitants of the Bieszczady Mountains, the number of such places may exceed 250 [17, 19].

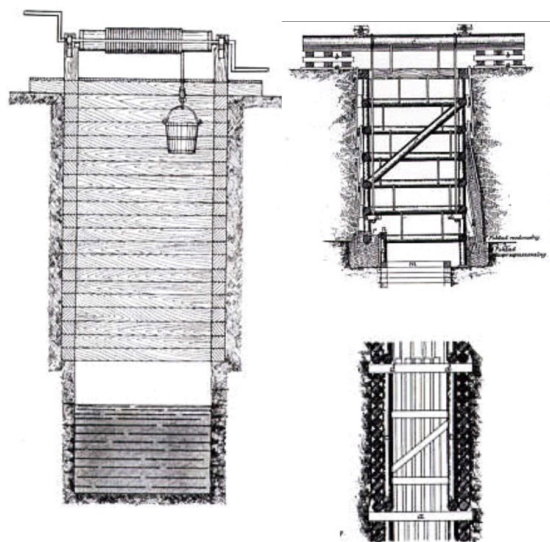


Fig. 3. Cross section of a hand-dug well with winch, timber lining [20 – modified]

The places of crude oil outflow and natural gas exhalation are also interesting from the scientific point of view, as evidenced by numerous articles and scientific studies [11, 12, 21–25].

The presence of volatile hydrocarbons within such facilities poses a serious risk of methane explosion, while hydrogen sulphide poisoning is also dangerous to the health and life of people residing there [11, 12].

In order to reduce the risk of ignition and/or explosion of methane or poisoning with hydrogen sulphide, people living in the potentially dangerous zone are obliged to be equipped with gas detectors, automatic notifying them of hazards by means of light and sound signals. Among these tools is the Dräger X-am 8000 [26, 27], which is portable and can at the same time measure the concentration of seven gases, including hydrogen sulphide and methane [26–28].

The occurrence of an explosion hazard generated while in the immediate vicinity of the excavation's outlet or an inactive borehole is related to the explosiveness of the air-gas mixture. Methane belongs to the gases whose emissions can be hazardous to human health and life [29, 30]. Methane is a flammable gas that reacts with oxygen, and the chemical reaction produces a flame accompanied by large amounts of heat. The ignition initiator for methane is, for example, a spark or

a flame. The combustion is explosive when the concentration of methane in the air is between the lower and upper explosive limits [31].

The explosion limits expressed by the content of Methane in a mixture with air at a temperature of 20°C and a pressure of 1 bar are [31]:

- 5% vol./vol. Methane – lower explosive limit (LEL),
- 15% vol./vol. Methane – upper explosive limit (UEL).

Ignition of methane may occur spontaneously if the temperature of its mixtures in the air reaches 537°C at a pressure of 1 bar [31, 32].

Methane is a colourless, odourless, and tasteless gas that is lighter than air. It burns with an almost colourless flame with a blue halo [31–33].

Methane is not a toxic gas. This gas in high concentration has a suffocating effect on the respiratory system and displaces oxygen. Poisoning with this gas can even lead to unconsciousness, and in low concentrations it can cause narcotic effects [31–33].

Another gas that may appear in the air while in the immediate vicinity of the shaft exit or inactive borehole is hydrogen sulphide. This gas is classified both as to explosive gases and toxic. Exceeding the permissible concentration level may have a negative influence on human health and life [31, 32, 34].

Hydrogen sulphide is a colourless gas with a strong odour of rotten eggs, when the gas concentration exceeds 0.18 mg/m<sup>3</sup> [34]. When concentration of the gas ranges from 1400 to 2800 mg/m<sup>3</sup>, it may stop respiratory processes [34].

Hydrogen sulphide is a flammable and explosive gas. The explosive limits of the gas in the air mixture are given below [34]:

- 4.3% vol./vol. hydrogen sulphide – lower explosive limit (LEL);
- 45% vol./vol. hydrogen sulphide – upper explosive limit (UEL).

The self-ignition temperature of hydrogen sulphide in the air mixture is 290°C [34].

### 3. The Dräger X-am 8000 portable gas multi-detector. Features and types of sensors compatible with it

The Dräger X-am 8000 (Fig. 4) portable gas multi-detector is ATEX-certified. This means that it can be used in an area where an explosive mixture of gases, vapours or oxygen can be generated temporarily or continuously. This explosion hazard area is classified as zone 0 [26–28].



Fig. 4. List of the basic features in Dräger X-am 8000 [28 – modified]

The Dräger X-am 8000 is a modern multi-gas detector with a build-in, high performance pump for a simultaneous and continuous monitoring of up to seven gases [26–28].

The detector has five slots into which four types of sensors can be installed as required, including dual-use sensors. The device can be armed with the following sensors [26–28]:

- infrared,
- photoionization,
- catalytic,
- electrochemical in XXS version for measuring oxygen and toxic gases.

Thanks to this, it is possible to select from the pool of 42 sensors those corresponding to the current needs in an easy way. In total, it makes it possible to measure the concentrations of 124 gaseous substances [26–28, 35].

The device is also equipped with a Bluetooth module that allows X-am 8000 to communicate with other

systems or mobile devices with a dedicated application. This enables online data exchange or reading of measured values away from the gas sampling point [27, 28, 35].

### Infrared (IR) sensor – principle of operation

The gas sample is transferred to the measuring cuvette by diffusion or a pump. The infrared emitter produces broadband radiation that passes through the window into the cuvette, where it is reflected by mirrors and passes through another window, hitting the dual detector. The dual detector consists of a measuring detector and a reference detector. If the gas mixture contains, inter alia, hydrocarbons, then some of the radiation is absorbed and the measuring detector produces a reduced electrical signal. The signal from the reference detector remains unchanged [27, 35, 36]. The DrägerIR sensor principle is presented in Figure 5.

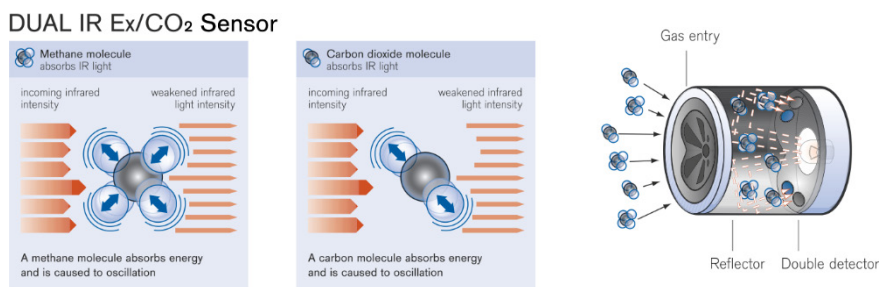


Fig. 5. Principle of infrared Dräger sensor [27 – modified]

## Photoionization detector (PID) – principle of operation

Gas particles are detected if, under the influence of radiation emitted by the UV lamp, are ionized, i.e. the ionization energy is lower than the energy emitted by photons. The presence of ionization products is recorded by an electrometer. The resulting ions recombine [27, 33, 35, 36]. The Dräger PID sensor principle is presented in Figure 6.

## Catalytic bead sensors – principle of operation

A small coil made of platinum is embedded in a porous ceramic bead with a diameter of less than 1 mm [27, 35, 36]. A current flows through the platinum coil, heating the pellistor above 100°C. When temperature of the pellistor will increase in the presence of flammable gases, it contains a suitable catalytic material, which leads to causes the resistance of the platinum coil to such an increase. This change in resistance can then be evaluated electronically. For combustion, pellistor uses oxygen from the ambient air [27, 35, 36]. This sensor works on the basis of the catalytic bead principle. A second pellistor is used with almost the same structure in order to eliminate changes in the ambient temperature. The second pellistor does not react to gas. Coupled by a Wheatstone bridge, the two pellistors then form a sensor circuit, which is largely independent of the ambient temperature, and which can detect the presence of flammable gases and vapours [27, 35, 36]. The Dräger Catalytic bead sensor principle is presented in Figure 8.

## Electrochemical sensor – principle of operation

The basic principle of an electrochemical sensor is that at least two electrodes (the measuring electrode and the counter electrode) are in contact with each other in two ways: first, through an electrically conductive medium (electrolyte), and second, through an external electrical circuit (electron conductor). The electrodes are made of a material with catalytic properties, thanks to which chemical reactions take place in the so-called three-phase zone [27, 35, 36]. The Dräger Electrochemical sensor principle is presented in Figure 7.

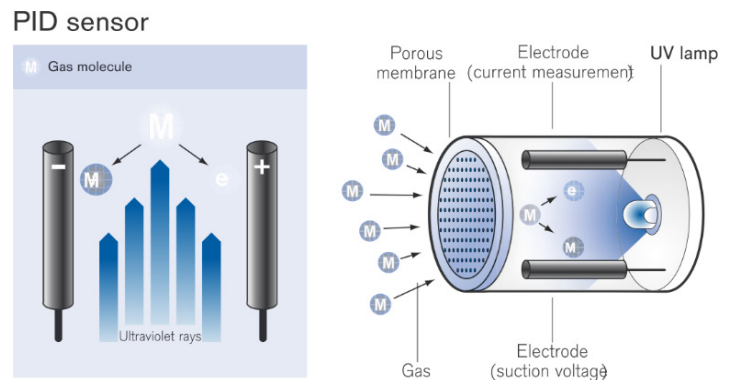


Fig. 6. Principle of photoionization detector – Dräger (PID) sensors [27 – modified]

## Electrochemical sensor

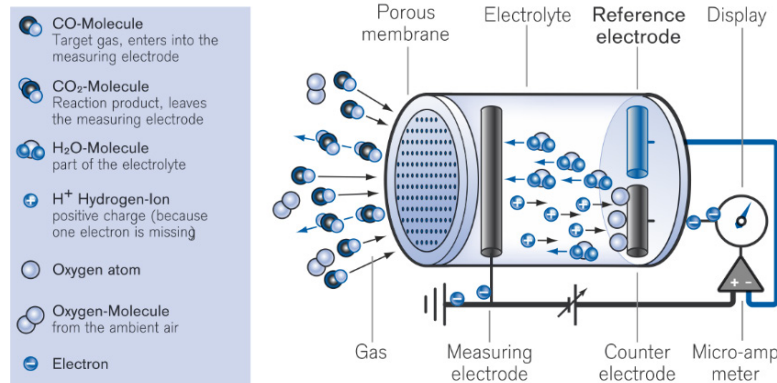


Fig. 7. Principle of electrochemical Dräger sensor [27 – modified]

### Catalytic bead sensors

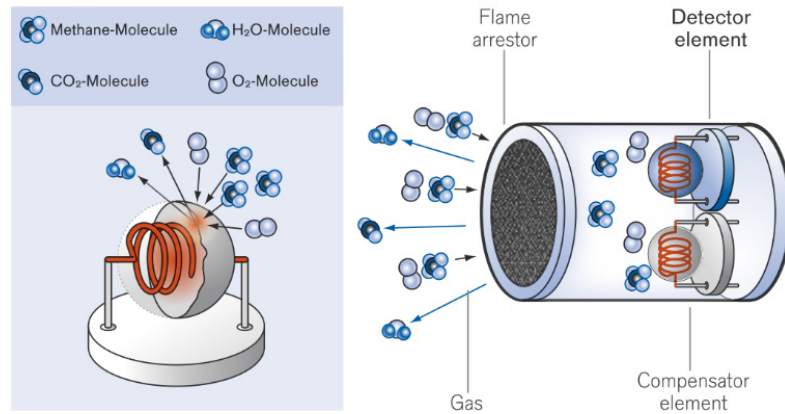


Fig. 8. Principle of catalytic bead Dräger sensors [27 – modified]

## 4. Use of the Dräger X-am 8000 for monitoring a gas mixture in the air within old oil and gas fields

In places where abandoned crude oil or natural gas fields occur, people there come into contact with liquids or gases classified as dangerous to human health or life and these substances can also pose a risk of ignition or explosion. At the time when work is performed in this area, in accordance with Polish law, the area should be

marked, properly secured, and monitored [33, 37–39]. In this case, the most effective, also in economic terms, type of monitoring is mobile monitoring.

The Dräger X-zone 8000 multi-gas detector can successfully perform this function and, in combination with the dedicated Dräger X-site Live set (Fig. 9), it is a tool for real-time monitoring of a potentially hazardous area for human life and health. The advantage of this combination is that the Dräger X-site Live kit weighs just over 10 kg and is the size of a suitcase. In addition, Dräger X-site Live is equipped with a mobile device through which one can observe the current indications of the gauges and reconfigure it [35, 40].



Fig. 9. Dräger X-site Live set contents [40 – modified]

In addition to the designated slot for the Dräger X-zone 8000 multi-gas detector, there are communication modules inside the case: GSM, GPS, Wi-Fi and Bluetooth. This enables real-time transmission of measurement data to any place on Earth [40]. Also in this way, the device transmits information about the existing threat to life or health. When one of the sensors registers the exceedance of the permissible value for each of the tested substances, the message about the danger is automatically sent to all active users who are in the monitored zone and remotely supervising the work. In addition to electronic notification, the Dräger X-zone 8000 and the Dräger X-site Live kit emit a warning flashing light, an audible alarm signal and vibration via the Dräger X-zone 8000 multi-gas detector [27, 28, 35, 40].

The oil and gas industry also uses radiation generators and radioactive sources. The radioactive materials used may also pose a potential threat to the natural environment and to humans [40, 41]. For radiation protection, Dräger X-site Live is also equipped with a gamma detector with an alarm set at 50  $\mu\text{m}/\text{h}$  (0.5  $\mu\text{Sv}/\text{h}$ ). The measurement takes place in two seconds [40].

## 5. Conclusions

Old and abandoned oil and gas fields, in the form of pits and unprotected borehole outlets, may pose a risk of poisoning by escaping gases or lead to the ignition or explosion of methane.

The Dräger X-am 8000 portable multi-gas detector can be used to detect both toxic and explosive gases in the air.

Thanks to their mobility and technical parameters, the Dräger X-am 8000 together with Dräger X-site Live can be used for continuous and periodic monitoring of concentrations of up to 7 gases simultaneously, including explosive gases such as Methane and toxic gases such as e.g. Hydrogen sulphide.

Dräger X-am 8000 together with Dräger X-site Live can be used to monitor the concentration of gases in potentially explosive zone 0 during tourism or when carrying out, inter alia, research and inventory work related to zone protection.

Using communication modules in the Dräger X-site Live wireless hazardous area monitoring station, conditions in the workplace can be remotely monitored by the controllers.

Recognition of technical objects as monuments of a bygone era, appreciation of their cultural and artistic values contributes to the emergence and development of industrial tourism.

## Acknowledgements

The paper was written within the framework of statutory research at the Faculty of Drilling, Oil and Gas at AGH University of Science and Technology in Kraków, Poland No. 16.16.190.779.

---

## References

- [1] Kronenberg M.: *Wpływ zasobów dziedzictwa przemysłowego na atrakcyjność turystyczną miasta. Przykład Łodzi*. Wydawnictwo Uniwersytetu Łódzkiego, Łódź 2013.
- [2] Kruczek Z., Kruczek M.: *Post-industrial Tourism as an Opportunity for Revitalising the Environment of the Former Oil Basin in the Polish Carpathian Mountains*. Polish Journal of Environmental Studies, vol. 25, iss. 2, 2016, pp. 895–902.
- [3] World Tourism Organization: *International Tourism Highlights*. UNWTO, Madrid, Spain, 2019, pp. 1–24. DOI: <https://doi.org/10.18111/9789284421152>.
- [4] Augustyn B.: *Pamięć krajobrazu – przeszłość zapisana w teraźniejszości*, [in:] *Bojkowszczyzna zachodnia – wczoraj, dziś i jutro*, ed. J. Wolski, Vol. 2. Polska Akademia Nauk, Instytut Geografii i Przestrzennego Zagospodarowania im. Stanisława Leszczyckiego, Warszawa 2016, pp. 65–83.
- [5] Karpacki Trakt Naftowy. <https://www.gorlice.pl/pl/333/0/karpacki-trakt-naftowy.html> [16.06.2021].
- [6] Kruczek Z.: *Rola turystyki w zachowaniu dziedzictwa przemysłu naftowego w Polskich Karpatach*. Turystyka Kulturowa, vol. 3, 2019, pp. 33–52.
- [7] Małopolski Szlak Naftowy. <http://szlakimalopolski.mik.krakow.pl/?szlaki=szlak-naftowy> [16.06.2021].
- [8] Odkryj Podkarpackie. <https://podkarpackie.eu/turystyka/muzeum-przemyslu-naftowego-i-gazowniczego-w-bo-brce/> [16.06.2021].
- [9] Towarzystwo Opieki nad Zabytkami – Oddział Bieszczadzki. <http://www.tonzbieszczadzki.pl> [16.06.2021].
- [10] Cząstka J.: *Z dziejów górnictwa naftowego w Bieszczadach*. Nafta, vol. 6, 1961, pp. 173.

- [11] Lipińska E.J.: *Places of natural flow of oil and natural gas emissions in Podkarpackie*. Infrastructure and Ecology of Rural Areas, vol. 1, 2010, pp. 13–24.
- [12] Sechman H., Dzieniewicz M.: *Pomiary emisji metanu w wybranych rejonach polskich Karpat Zewnętrznych*. Geologia, vol. 35, iss. 41, 2009, pp. 129–153.
- [13] Staszic S.: *O Ziemiórództwie Karpatów i innych gór i równin Polski*. W Drukarni Jego Ces. król. Mości Rządowej, Warszawa 1815.
- [14] Maruta M., Mirek-Jonkicz E.: *The „Rock oil” at your fingertips: hydrocarbons’ signs at the surface in the Polish Carpathians Area*. Mineralia Slovaca, Geovestník, vol. 43, iss. 2, 2011, pp. 183.
- [15] *Jak zostałem szejkiem bieszczadzkim*. <https://zyciejestpiekne.eu/jak-zostałem-szejkiem-bieszczadzkim> [16.06.2021].
- [16] Nowiny24: *W Bieszczadach tryska ropa*. <https://nowiny24.pl/w-bieszczadach-tryska-ropa/ar/c3-6010223> [16.06.2021].
- [17] *Przewodnik po Bieszczadach „Nieodkryte Bieszczady istnieją naprawdę”*. <https://wydawnictwo.lesneoko.com> [16.06.2021].
- [18] *Twoje Bieszczady*. [http://www.twojebieszczady.net/piesze/kopalnia\\_ropy.php](http://www.twojebieszczady.net/piesze/kopalnia_ropy.php) [16.06.2021].
- [19] Kuśmierk J., Dzieniewicz M., Sechman H., Machowski G., Czwarciel P., Maruta M., Ozimek K., Pałkowska K., Pasternacki A.: *Studium geologiczno-naftowe wycieków węglowodorów w rejonie Karpat*. Stowarzyszenie Naukowo-Techniczne Inżynierów i Techników Przemysłu Naftowego i Gazowniczego, Archiwum KSE AGH, Kraków 2007 [unpublished].
- [20] *Muzeum naftového dobývání a geologie z.s.* <http://muzeumropy.cz> [16.06.2021].
- [21] Guzy P., Pietrzycki D., Świerczewska A., Sechman H., Twaróg A., Góra A.: *Emission measurements of geogenic greenhouse gases in the area of “Pusty las” abandoned oil field (Polish Outer Carpathians)*. Journal of Ecological Engineering, vol. 18, iss. 4, 2017, pp. 100–109.
- [22] Kuśmierk J., Machowski G.: *Wycieki ropy naftowej w obszarze wschodniej części Karpat polskich i ich znaczenie prognostyczne*. Prace Instytutu Nafty i Gazu, vol. 150, 2008, pp. 247–250.
- [23] Maćkowski T., Kuśmierk J., Reicher B., Baran U., Kosakowski P., Łapinkiewicz A.P., Machowski G., Papiernik B., Szczygieł M., Zając A., Zych I.: *Dwuwymiarowe modele termicznego przeobrażenia materii organicznej i ekspulsji węglowodorów w transgranicznej strefie Karpat polsko-ukraińskich*. Geologia, vol. 35, iss. 4/1, 2009, pp. 191–222.
- [24] Maruta M., Sala D.: *Naturalne wycieki ropy naftowej a środowisko naturalne w Karpatach – wstępne wyniki badań*, [in:] *Interdyscyplinarne zagadnienia w górnictwie i geologii*, red. J. Drzymała, W. Ciężkowski, Oficyna Wydawnicza Politechniki Wrocławskiej, Wrocław 2013, pp. 119–127.
- [25] Sechman H., Guzy P., Kaszuba P., Wojas A., Machowski G., Twaróg A., Masłanka A.: *Direct and indirect surface geochemical methods in petroleum exploration: a case study from eastern part of the Polish Outer Carpathians*. International Journal of Earth Sciences, vol. 109, 2020, pp. 1853–1867, DOI: doi.org/10.1007/s00531-020-01876-y.
- [26] Dräger: *Measurement strategy: Dräger X-am 8000 with PID-Sensor*; Dräger Safety AG & Co. KGaA, Lübeck, Germany, 2017, pp. 1–4.
- [27] Dräger: *Dräger Sensor® & Portable Instruments Handbook*. 4<sup>th</sup> ed., Dräger Safety AG & Co. KGaA, Lübeck 2018.
- [28] Dräger: *Dräger X-am® 8000 Multi-Gas Detector*. Drägerwerk Safety AG & Co. KGaA, Lübeck 2021.
- [29] Kissell F.N.: *Handbook for Methane Control in Mining*. Information Circular/2006, NIOSH – Publications Dissemination, Cincinnati 2006.
- [30] Solecki T., Macuda J.: *Metody wykrywania i identyfikacji substancji ropopochodnych w środowisku gruntowo-wodnym*. Wiertnictwo, Nafta, Gaz, vol. 21, iss. 1, 2004, pp. 325–332.
- [31] Krawczyk M.: *Analityka procesowa – wybuchowość mieszanin gazowych, czujniki chemiczne do pomiaru wybuchowości*. Wykład. Gdańsk 2003 [unpublished].
- [32] *Safety Data Sheets*. <https://przemysl.air-liquide.pl/en/resources/safety-data-sheets> [16.06.2021].
- [33] Smolarz A.: *Diagnostyka procesów spalania paliw gazowych, pyłu węglowego oraz mieszaniny pyłu węglowego i biomasy z wykorzystaniem metod optycznych*. Politechnika Lubelska, Lublin 2013.
- [34] Stetkiewicz J.: *Siarkowodór. Dokumentacja dopuszczalnych wielkości narażenia zawodowego*. Podstawy i Metody Oceny Środowiska Pracy, vol. 4 (70), 2011, pp. 97–117.
- [35] Dräger: *Portable gas detectors – Product overview*. Dräger Safety AG & Co. KGaA, Lübeck 2020.
- [36] Dräger: *Wprowadzenie do detekcji gazów*. Dräger Safety AG & Co. KGaA, Lübeck 2016.
- [37] *Obwieszczenie Ministra Gospodarki, Pracy i Polityki Społecznej z dnia 28 sierpnia 2003 r. w sprawie ogłoszenia jednolitego tekstu rozporządzenia Ministra Pracy i Polityki Socjalnej w sprawie ogólnych przepisów bezpieczeństwa i higieny pracy*. Dz.U. 2003, nr 169, poz. 1650.
- [38] *Rozporządzenie Ministra Gospodarki z dnia 25 kwietnia 2014 r. w sprawie szczegółowych wymagań dotyczących prowadzenia ruchu zakładów górniczych wydobywających kopaliny otworami wiertniczymi*. Dz.U. 2014, poz. 812.

- [39] *Rozporządzenie Ministra Gospodarki z dnia 8 lipca 2010 r. w sprawie minimalnych wymagań, dotyczących bezpieczeństwa i higieny pracy, związanych z możliwością wystąpienia w miejscu pracy atmosfery wybuchowej.* Dz.U. 2010, nr 138, poz. 931.
- [40] *Dräger: X-site Live – Wireless hazard area monitor.* Drägerwerk Safety AG & Co. KGaA, Lübeck 2021.
- [41] *International Atomic Energy Agency (IAEA): Radiation protection and the management of radioactive waste in the oil and gas industry.* Safety Reports Series, No. 34, International Atomic Energy Agency, Vienna 2003.





Magdalena Sowa-Zyzańska

AGH University of Science and Technology  
ORCID: 0000-0003-4685-1436

## ELEMENTS OF RESERVOIR SIMULATION FOR TIGHT GAS RESERVOIRS WITH WATER INFLUX

Date of submission:  
28.06.2021

Date of acceptance:  
29.06.2021

Date of publication:  
31.08.2021

© 2021 Author. This is an open access publication, which can be used, distributed, and reproduced in any medium according to the Creative Commons CC-BY 4.0 License

<https://journals.agh.edu.pl/jge>

**Abstract:** At present, gas obtained from unconventional deposits plays an important role in the global economy as an energy factor. The simulation of the exploitation of this type of deposits is very complex and requires an individual approach for each case, which is extremely inspiring and interesting, therefore this article attempts to deal with the problem of modeling the extraction of natural gas from tight unconventional deposits. Extraction of tight gas requires the use of measures that stimulate this process and requires an unusual approach both at the stage of deposit recognition, its drilling and exploitation. Using computer programs, more and more accurate models are developed taking into account almost all known processes occurring in the deposits during exploitation, which significantly influences the better selection of parameters of wells and operations that intensify the production, and thus improves the results of exploitation.

**Keywords:** tight gas, reservoir simulation, water influx, hydraulic fracturing

---

# 1. Introduction

Crude oil and natural gas are energy resources of tremendous economic and political importance, both for highly developed and poor countries, which have these raw materials in quantities that allow them to create a market, as well as for countries that do not have hydrocarbon resources or have small amounts at their disposal. Therefore, over time, new gas deposits are sought in structures that were previously not of interest. Both during the exploration and their subsequent exploitation, there are problems that must be defined and solved. Therefore, over the years, the following deposits have been distinguished, i.e. the natural accumulation of hydrocarbons in the rocks as: conventional, i.e. those that can be exploited through boreholes without additional technical and technological treatments aimed at intensifying extraction, and unconventional ones – requiring specialized treatments and an individual approach, without obtaining the raw material would be insignificant, and thus unprofitable [1].

Among the terms that have emerged in connection with the search for gas in unconventional structures is the term “closed gas”. The term is commonly used to refer to structures with low permeability in which natural gas is trapped. In the 1970s, the concept of tight gas was defined and standardized by the government in the United States. The US Natural Gas Policy Act (NGPA, Public Law 95–621) of 1978 classifies tight gas fields as structures with a permeability of less than 0.1 mD. This definition, according to the sources, was a political definition and was used to determine which wells would receive federal and/or state tax credits for gas production. Today, this definition is a function of many physical and economic factors. Another definition of tight natural gas deposits, which is considered the best at present, is the definition of gas tight in a rock structure, and its extraction is not possible on an economically justified level without performing intensification procedures, such as e.g. hydraulic fracturing. Additionally, it is justified to make horizontal holes, including branched wells [2].

In order to properly classify a newly discovered natural gas deposit, it is necessary to characterize the deposit parameters. Important geological parameters that should be investigated and determined for the stratigraphic unit in question include: the spatial arrangement of the deposit, the type of genetic facies, textural maturity, mineralogy, diagenetic processes, dimensions of the structure and the occurrence of natural fractures in the rock. One of the most difficult parameters to evaluate for a tight gas field is the size and shape of the drainage zone. These types of structures show constant pressure disturbances even after

long periods of operation (months or even years). When the drainage zone takes an oblong shape, it may indicate the presence of natural fractures in the rock or the presence of hydraulic fractures during the treatment. The drainage zone in this type of deposit largely depends on the number of drilled holes and the number, method and quality of fracturing treatments. The pressure and temperature rise are abnormally high due to the considerable depth of the gas-bearing layers. Other important parameters strongly related to the petrophysical description of the deposit are: rock porosity and permeability. From the point of view of tight gas deposits, it is important that the pore space distribution in the deposit rock is largely regular, and the porosity in this type of sandstone usually ranges from 2% to 12% [3]. Pores are usually poorly connected, which is caused by numerous diagenetic processes generating, for example, an increase in quartz, which in turn significantly impedes gas exploitation, as well as easy gas flow to the borehole. For this reason, the permeability of these rocks also reaches low values, which causes a rapid drop in extraction during exploitation. Natural cracks in the rock structure are a positive aspect that enables the exploitation of tight gas. Moreover, rocks forming tight gas deposits are usually thicker (in the order of several hundred meters) than those of conventional deposits.

Saturation of the deposit rock with bound water is another important parameter in the process of identifying and modeling hydrocarbon extraction from a tight gas deposit. There are several problems with the analysis of this parameter. In the first place, bound water saturation in rocks of this type is usually quite high, although it can vary depending on the type of rock, and is also irreducible [4]. Sandstones, classified as conventional formation rocks, exhibit an irreducible bound water saturation of between 15% and 20%. Compact gas-bearing sandstones have higher water saturation values – approx. 40%, and thus also a higher capillary pressure. On the other hand, for example, shale and siltstones show the highest irreducible water saturation – over 60% and thus high capillary pressure. Compact gas-bearing sandstones, despite high water saturation, often still accumulate gas that is “free” of water. This property plays a particularly important role when the gas-saturated part of the bed is accompanied by a water-saturated zone. Depending on the size of this zone, the amount of water saturation of the deposit rock, the wettability of the rock surface with water, the surface tension at the phase boundary, as well as the amount of hydraulic resistance of water flow in the analyzed porous medium, the inflow of water to the deposit poses a potential threat to the mining process. This zone may occupy most of the deposit, leading to the movement of water in the

direction of the borehole, resulting in the formation of, for example, a water cone. In order to avoid or limit the consequences associated with this unfavorable phenomenon, reservoir engineering is to determine the maximum efficiency for which gas is exploited without water (the fluid flow towards the well is single-phase) [4].

## 2. Method section

To create the base simulation model, the author used the CMG GEM (GEM – Generalized Equation of State Model) software – a compositional simulator (in the academic version) operating on the basis of an adaptive implicit scheme developed by Thomas and Thurana and Collins et al.

The construction of the batch file began with the determination of the area of an exemplary deposit. At this stage, the author did not have data from the real deposit. The assumed area of the deposit is a 1500 m × 1500 m saturated with high-methane gas. The assumed thickness of the structure saturated with gas is 40 m, and the zone saturated with the underlying water has a thickness of 30 m. It was assumed that the structure was homogeneous. The assumed depth of the top of the deposit is 4500 m, and the depth of the aquifer is 4540 m. The temperature of the deposit was set at 60°C, while the initial pressure was set at 50 MPa. This pressure is 10% higher than the hydrostatic pressure, which is a phenomenon characteristic of tight gas deposits (anomalously high reservoir pressure) [3]. One of the initial elements defined in the batch file creation phase in Builder is to define the dimensions of the block grid for the subsequent calculation process. The correct selection of the mesh is an extremely important element, as it determines to a large extent not only the accuracy of the results, but also the possibility of creating calculation variants. Considering the time-consuming nature of the simulation, the number of blocks should be minimized (the CMG GEM academic license, which was used to carry out this part of the work, allows to create a maximum of 1000 blocks), which in turn maximizes their dimensions to meet the initial assumption of the dimensions of the deposit. On the other hand, smaller block dimensions give more accurate calculation results, which is of particular importance when analyzing, for example, hydraulic fracturing of boreholes and determining the impact of deposit water activity on the course of exploitation. Therefore, in the base model, the dimensions of blocks in the X-Y plane were assumed to be 50×50 m. The vertical dimensions of the blocks were varied so that the smallest dimensions

were closest to the gas-water contour, which will allow for more accurate results regarding the amount of water flowing into the deposit from the aquifer during the simulation. Such assumptions led to the separation of 7 layers in the model (Tab. 1). The model uses a Corner Point mesh. Keeping the area of the modeled deposit area assumed at the beginning, the number of blocks in each direction is arranged as follows: in the x-axis direction – 30, in the y-axis direction – 30, in the z-axis direction – 7, blocks equal to 6300. For the entire model, a constant value of porosity equal to 6% and the horizontal permeability – 0.05 mD, while the vertical permeability was adopted at the level of 10% of the horizontal permeability.

**Table 1.** Comparison of the thickness values of individual layers of the simulation model

Layer	Volume [m]
1	15
2	10
3	10
4	5
5	5
6	10
7	15

Another section defined in the process of creating the simulation model is determining the parameters of the reservoir fluid. A simplified gas-water model was adopted. The values of individual parameters are collected in Table 2, while the remaining ones needed calculations that were generated using correlations that are part of the software used.

**Table 2.** List of values of PVT model parameters

Parameter	Value	Unit
Temperature	60	[°C]
Gas density	0.697	[kg/m <sup>3</sup> ]
Water density	1075	[kg/m <sup>3</sup> ]
Water volume coefficient in relation to initial pressure	1.02395	[-]
Water compressibility ratio	4.62·10 <sup>-7</sup>	[1/kPa]
Pressure at standard conditions	101.325	[Kpa]
Water viscosity	0.421	[cP]

An important part of the model is the preparation of phase permeability plots. In this case, they were created based on the two-phase gas-water correlation in moderately wettable sandstone with interfacial. The assumed values of characteristic points are presented in the diagrams Figure 1.

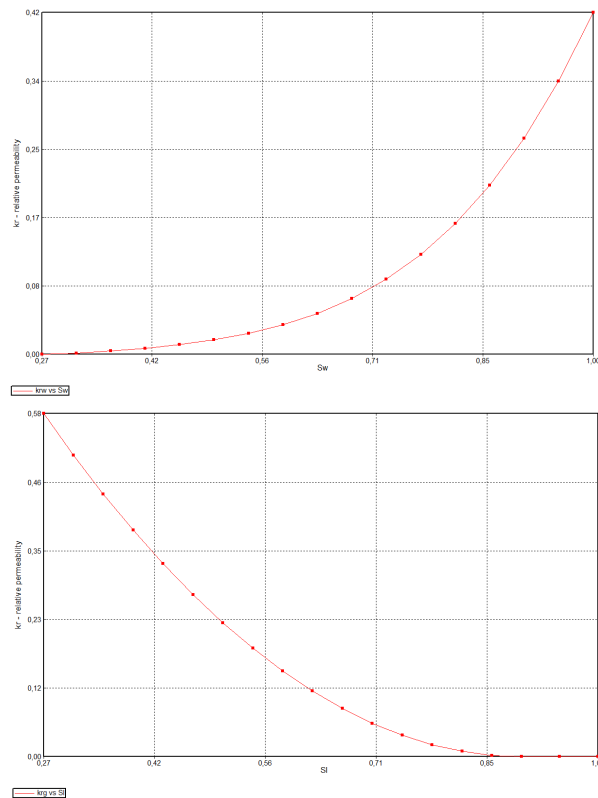


Fig. 1. Relative permeability curves as a function of fluid saturation

For all variants, it was assumed for comparison that the gas would be operated with a maximum initial expenditure of 150,000 nm<sup>3</sup>/day. The operating time was assumed to be 30 years, with a time step of one year.

### 3. Results

The created base model was used to generate various exploitation variants. In the calculations, the author analyzed the following variants: mining with a vertical, horizontal well (and within these variants, the impact of the location of the well in the deposit and the available volume of the deposit were analyzed), as well as mining with a hydraulically fractured vertical well and a horizontal well-fractured well. In the variants with the use of the fracturing treatment, not only the impact of the location of the borehole or the available thickness was examined, as in the case of without the use of fracturing, but also the impact of individual fracturing parameters on the operation process, as well as the impact of the initial size of the drilling expenditure on gas and water production over time.

For the assumed variants, a simulation of the course of reservoir fluid extraction was carried out in order to compare the effectiveness of the operation of a vertical and horizontal well, to evaluate the effectiveness of the hydrau-

lic fracturing treatment, as well as to analyze the impact of well parameters such as: well depth, deposit thickness made available by the well, as well as fracturing parameters such as such as the fracture permeability, the length of the fracture wing (impact range) or the number of fractures made in the case of horizontal wells. On the basis of the simulations, the most interesting aspect was the influence of hydraulic fracturing parameters on the exploitation process, therefore the results obtained for this variant will be presented in the further part of the article.

#### 3.1. Horizontally drilled horizontal wells

For a horizontal well fractured several times, the impact of changes in the length of the fracture wing, permeability and the number of fractures in the horizontal section on the mining process was analyzed. The calculations assume the length of the fissure wing (for  $x$ : 50; 100; 150; 200; 250 m) and the permeability ( $k$ : 1; 5; 10; 20; 50 D), but also the number of gaps: 5; 8; 10; 12. The following parameter values were adopted in the reference model: number of gaps equal to 10, wing length  $x_{ref}$  equal to 150 m and permeability  $k_{ref}$  5 D.

In order to improve the quality of the calculation results, the author adapted the block grid. The dimensions

of the blocks  $25 \times 25$  m were assumed closest to the well, and as they moved away from the well, the dimensions were doubled, resulting in a deposit area of  $1100 \times 2800$  m, which gives the number of blocks equal to 6.426. Simulating only one wing of the slot. Such a procedure allows to obtain a larger impact zone of the well and more accurate simulation results, and due to the symmetry running along the horizontal section of the well, which is 1000 m, the obtained results of the quantity of extracted formation fluids can be multiplied by two, obtaining the same results as for the operation of both wings Figure 2.

The first analyzed parameter was the distribution of hydraulic fractures in the stimulated zone. On the basis of the analyzed variant results, it was found that the number of hydraulic fractures made should be selected in such a way as to ensure effective drainage of the stimulated zone, while avoiding overlapping zones of adjacent fractures. Planning too many fractures in close proximity causes the parameters of the fracturing treatment to deteriorate.

Figure 3 presents the profiles of efficiency and total gas extraction for the proposed variants, while Figure 4 presents changes in water extraction depend-

ing on the variant. Based on the charts and results presented in Table 3, the following relationship was observed: with the increase in the density of hydraulic fractures, the production of natural gas and water increases, and the increase is greater for water. In the case with the smallest number of fractures, gas production is 7.2% lower than in the reference variant (10 fractures), while for water it is 31.41% lower. For the variant with the largest number of fractures, gas production increased by only 2.92%, and water by as much as 47.01%. As can be seen from diagram Figure 3, the impact of the arrangement of the fractures is of key importance on the production of gas in the initial stage of exploitation, then the greatest differences in expenditure are observed, moreover, the greater the number of fractures, the longer the production remains with the given initial expenditure. However these differences then fade away. The opposite is true, however, in the case of extracted water, in the first years of exploitation the amount of extracted water is similar in each variant, and the greatest differences are observed in the last year of extraction.

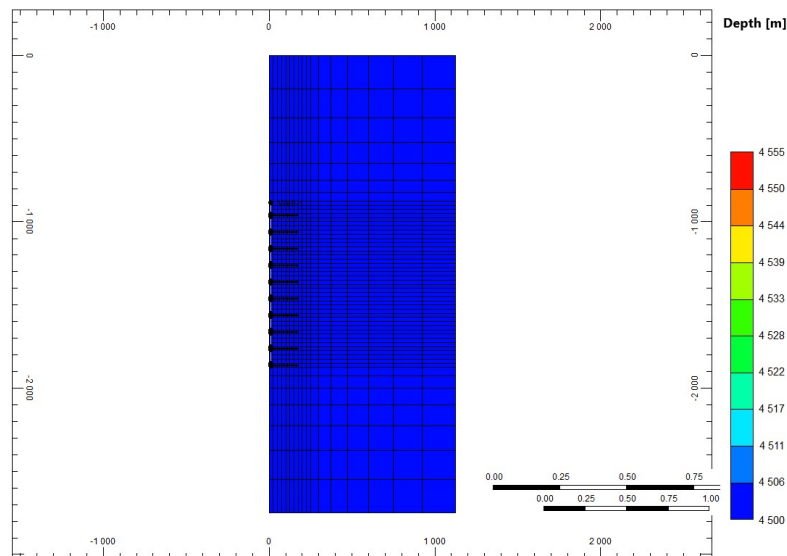


Fig. 2. Location of the horizontal well along with hydraulic fracturing in the model – reference model

Table 3. Summary of the results of the analysis of the influence of the number and distribution of hydraulic fractures on the course of exploitation

Number of hydraulic fractures	Total gas extraction [ $10^6 \text{ m}^3$ ]	Difference in extraction relative to reference values [%]	Total water extraction [ $10^3 \text{ m}^3$ ]	Difference in extraction relative to the reference value [%]
5	1973.44	-7.20	31.27	-31.41
8	2093.2	-1.57	44.6	-2.16
<b>10</b>	<b>2126.6</b>	-	<b>45.58</b>	-
12	2188.6	2.92	67.01	47.01

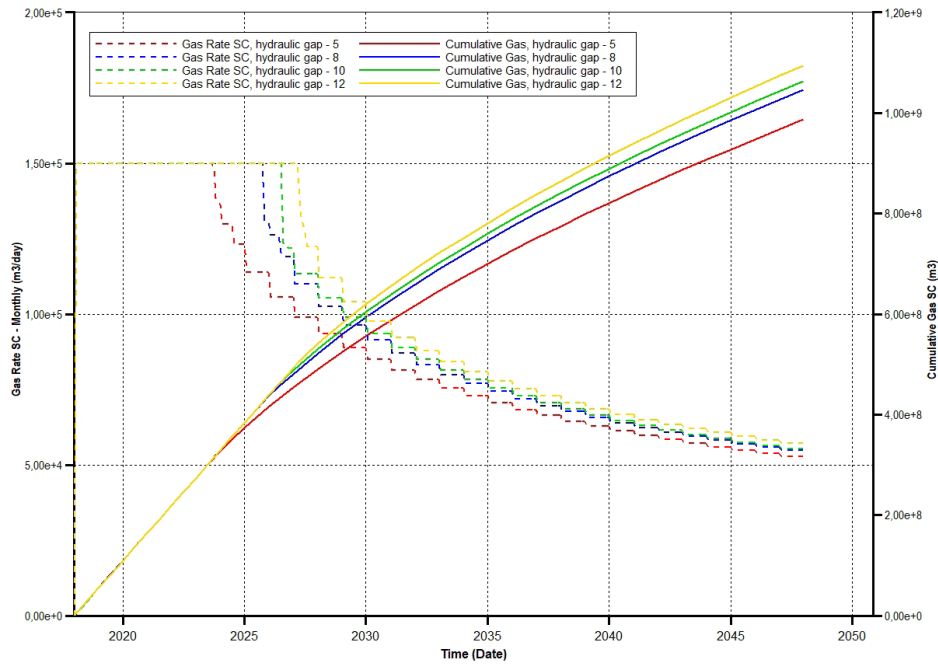


Fig. 3. Profiles of efficiency and total gas production depending on the number of hydraulic fractures (green – base value)

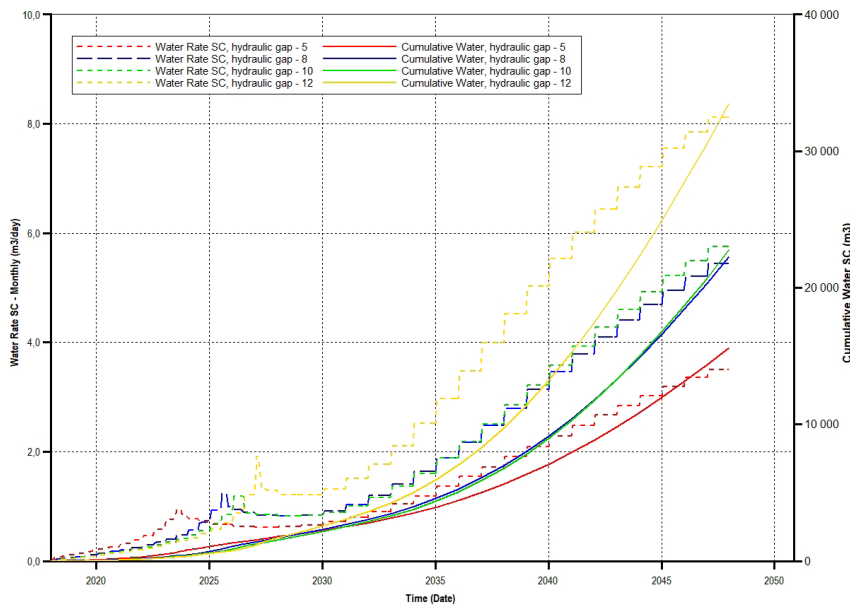


Fig. 4. Performance and total water extraction profiles depending on the number of hydraulic fractures (green – base value)

Another important parameter influencing the efficiency of hydraulic fracturing is the range of impact of this treatment. As part of this analysis, five fissure wing lengths were examined. The assumed range in this case was between 50 and 250 m with a step of 50 m. The simulation results are summarized in Table 4 and in the graphs Figures 5 and 6 on the basis of which it was

found that the production of gas and water from the deposit increases with the increase of the wing length. The longer the range of the slot wing, the longer the initially assumed gas flow is maintained. The differences in the flow of gas and water over time depending on the variant are similar to the arrangement of the slots in the well.

**Table 4.** Summary of results of the analysis of the impact of the range of hydraulic fractures on operation

Range of the hydraulic gap wing $x_{hf}$ [m]	Total gas extraction [ $10^6$ m <sup>3</sup> ]	Difference in extraction relative to reference values [%]	Total water extraction [ $10^3$ m <sup>3</sup> ]	Difference in extraction relative to reference values [%]
50	1823.16	-14.27	41.53	-8.89
100	1987.78	-6.53	49.18	7.90
<b>150</b>	<b>2126.6</b>	-	<b>45.58</b>	-
200	2251.6	5.88	39.33	-13.72
250	2380.6	11.94	33.78	-25.90

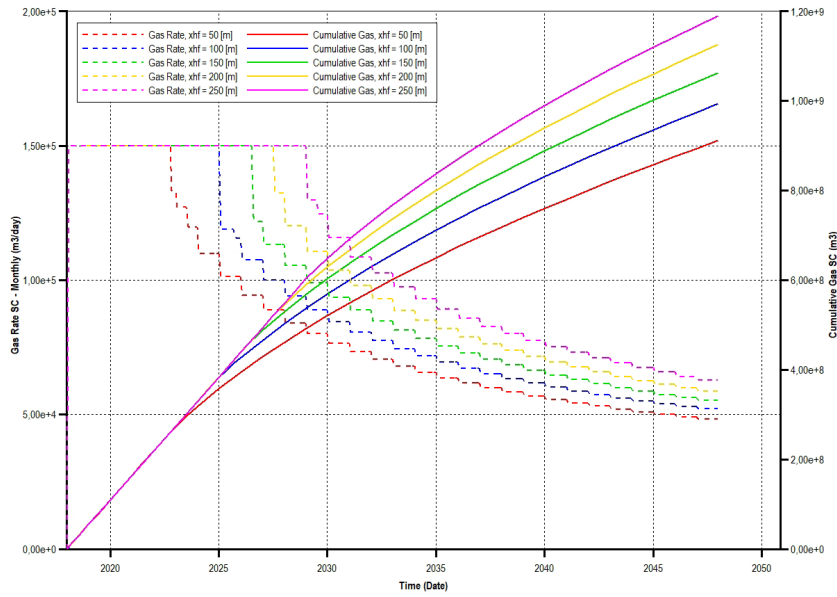


**Fig. 5.** Profiles of efficiency and total gas extraction depending on the range of hydraulic fractures in the range of 50–250 m (green – base value)

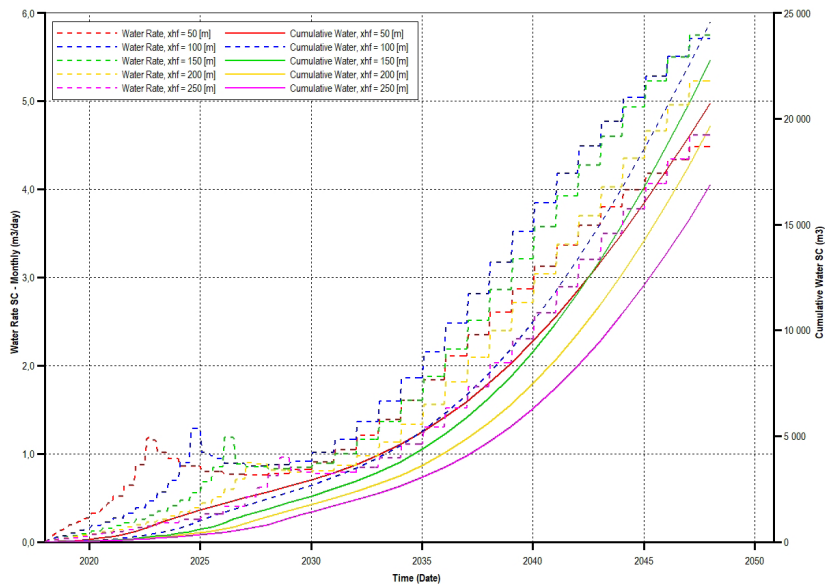


**Fig. 6.** Performance and total water extraction profiles depending on the range of hydraulic fractures in the range of 50–250 m (green – base value)

Analyzing the impact of hydraulic fracture permeability on the work efficiency of the well on basis of the obtained simulation results collected in Figures 7 and 8 as well as in Table 5, it can be concluded that it is much smaller than in the case of changes in the length of the fracture wing. There is a slight increase in gas extraction of, only 8.02%, with the fracture permeability of 50 D. However, it plays a significant role in the amount of water extracted. For the same case, an increase in water extraction by 142.57% compared to the reference variant was observed. The best fluid-conducting capac-

ity of hydraulic fractures is generated at the beginning of the service life, then the gas and water supply is the most intense, so at this time the fractures with the highest permeability will be able to deliver fluid to the well with sufficient capacity, but at a later time the difference between reservoir rock permeability and the hydraulic fracture permeability is so great that even fractures with weaker permeability will be able to deliver fluid to the wellbore with a sufficient flow. Therefore, the design of fractures with high permeability is unjustified in the context of the entire operation.

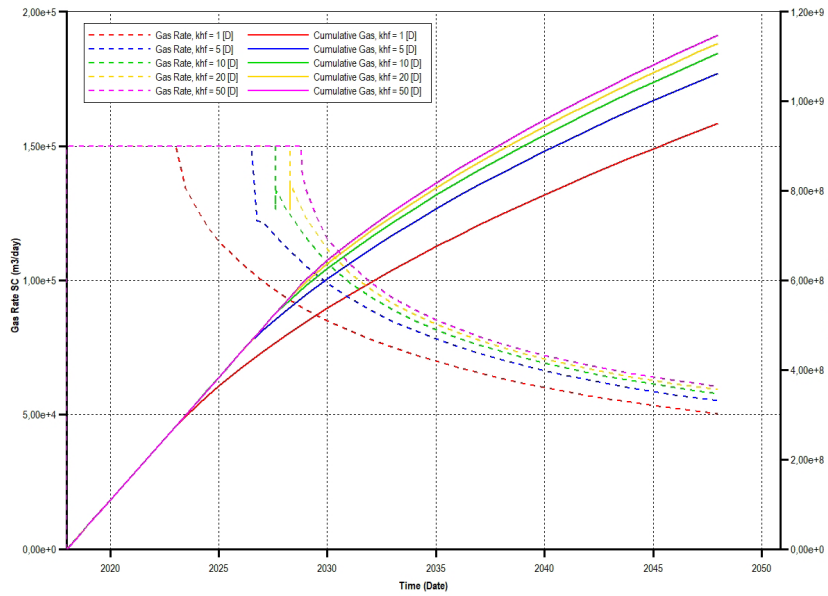


Fig. 7. Performance and total gas extraction profiles depending on the permeability of hydraulic fractures in the range of 1–50 D (blue – base value)

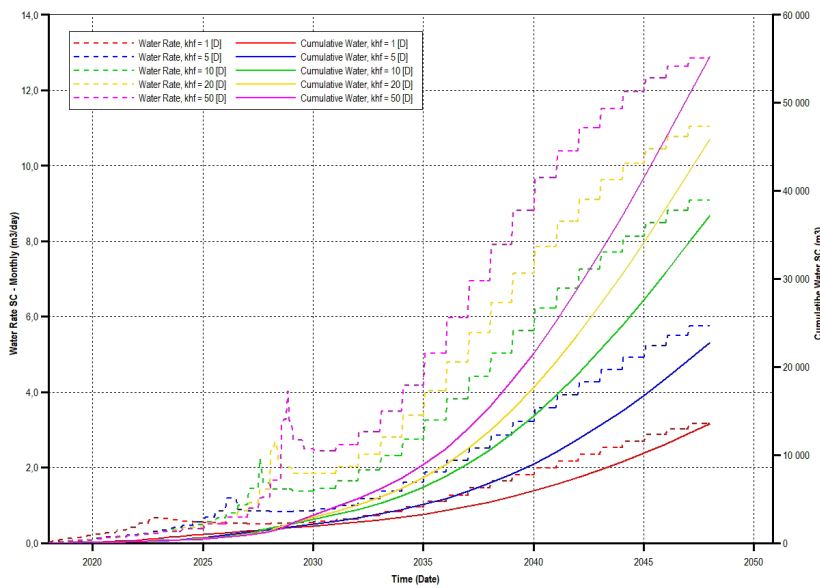


Fig. 8. Performance profiles and total water extraction depending on the permeability of hydraulic fractures in the range of 1–50 D (blue – base value)

**Table 5.** Summary of the results of the impact of the hydraulic gap permeability on operation

Permeability of hydraulic fractures $k_{hf}$ [D]	Total gas extraction [ $10^6 \text{ m}^3$ ]	Difference in extraction relative to reference values [%]	Total water extraction [ $10^3 \text{ m}^3$ ]	Difference in extraction relative to reference values [%]
1	1901.02	-10.61	27.05	-40.66
<b>5</b>	<b>2126.6</b>	-	<b>45.58</b>	-
10	2214.4	4.13	74.51	63.47
20	2260.4	6.29	91.84	101.48
50	2297.2	8.02	110.57	142.57

## 4. Discussion

The article presents a simulation model which is a numerical image of a fragment of an exemplary deposit with petrophysical parameters characteristic of a tight gas structure. The parameter values were adopted based on the collected literature. Additionally, the author defined the underlying layer in the base model. The author performed calculations for the variants mentioned in the article.

When designing a hydraulic fracturing treatment, basic parameters are selected such as: the range of the fracture wing, fracture permeability, and for a horizontal well, additionally the location of fractures on the horizontal section of the well. Therefore, the impact of changing individual parameters on the production was assessed. The analysis of the obtained results of the total gas production after 30 years of operation shows that the longer the fracture wing, the greater the production, but this relationship is true only up to a certain upper limit of the fracture length, different for different variants (depending on the location of the well in relation to the aquifer and the available thickness). This is due to a significant difference in the parameters of the zone covered by fracturing and the rest of the deposit, and the selection of better and better parameters of this treatment does not give the desired effects, because the gas flowing between the narrow fractures is not able to replenish the zone near the well so quickly. This leads to a sharp drop in pressure at the wellbore and, consequently, to cessation of operation until the pressure is rebuilt. The same is also true of gap permeability. The greater the permeability of the fracture, the more gas is able to flow into the well in a shorter time. However, the improvement of the gas flow conditions covers only the area of the fracture range and in the case of the analysis of this parameter, the rapid pressure drop, which was also observed in the fracture wing length analysis, is even more visible with the increase in fracture permeability. In some embodiments, this led to such a large pressure difference between the bed

and the zone around the wellbore that operation was only possible for a few days. The relationship is also true for the number of slots in a horizontal well, but in this case, when selecting an appropriate variant, the interaction of individual slots should be taken into account. If the gaps are located too close to each other, the effects of this treatment overlap. Such a solution has the opposite effect, leading to a deterioration of the operating results. In addition, the implementation of each additional gap generates a greater cost of the entire procedure.

Another aspect considered in the article was the amount of water flowing into the well. As for gas, the volume of water extraction is influenced by individual fracking parameters. The selection of appropriate fracking parameters and the location of the well in the reservoir can be the basis for limiting water extraction from the reservoir and preventing the formation of water cones.

## 5. Conclusion

To sum up, the specificity of tight gas deposits requires an individual approach to each newly discovered deposit at the stage of its modeling. The use of mining intensification procedures significantly complicates this process, however, it is necessary to obtain satisfactory results, as evidenced by both industrial practice and the obtained research results. Observing the behavior of the constructed deposit model when a horizontal well is operated with a fracturing treatment performed, it can be concluded that the most effective operation is a well with average parameters such as those adopted in the reference model, providing a small deposit area that will be exhausted as much as possible. At the same time, an appropriate network of wells should be created, which will have a slight interaction with each other, thanks to which effective gas extraction from the deposit will be achieved.

## References

- [1] Holditch S.A.: *Tight gas sands*. SPE 103356, 2006.
- [2] Siemek J., Nagy S.: *Energy carriers use in the world: natural gas – conventional and unconventional gas resources*. Archives of Mining Sciences, vol. 57, 2012, pp. 283–312.
- [3] Kiersnowski H., Buniak A., Kuberska M.: Srokowska-Okońska A.: *Występowanie gazu ziemnego zamkniętego w piaskowcach czerwonego spągowca Polski*. Przegląd Geologiczny, vol. 58, nr 4, 2010, pp. 335–346.
- [4] Papiernik B., Górecki W., Pasternacki A.: *Wstępne wyniki modelowań przestrzennych (3D) parametrów petrofizycznych skał podczas poszukiwań stref występowania gazu zamkniętego w polskim basenie czerwonego spągowca*. Przegląd Geologiczny, vol. 58, nr 4, 2010, pp. 335–346.
- [5] U.A. Congress, Office of Technology Assessment: *U.S. natural gas availability: gas supply through the year 200*, OTA-E-245, 1985.
- [6] Garcia J.P., Pooladi-Darvish M., Brunner F., Santo M., Mattar L.: *Well Testing of Tight Gas Reservoirs*. SPE-100576-MS, 2006.
- [7] Cox S.A., Gilbert J.V., Sutton R.P., Stoltz R.P.: *Reserve Analysis for Tight Gas*. SPE-78695-MS, 2002.
- [8] Poprawa P., Kiersnowski H.: *Związłe formacje zbiornikowe (tight reservoir) dla gazu w Polsce*. Biuletyn PIG, vol. 439, 2010, pp. 173–180.
- [9] Holditch S.A., Zee Ma Y.: *Unconventional Oil and Gas Resources Handbook: Evaluation and Development*. Elsevier Science, USA, 2016.
- [10] Wójcicki A., Kiersnowski H., Dyrka I., Adamczak-Biały T., Becker A., Głuszyński A., Janas M., Kozłowska A., Krzemiński L., Kuberska M., Paczeńska J., Podhalańska T., Roman M., Skowroński L., Waksmundzka M.I.: *Progностyczne zasoby gazu ziemnego w wybranych zwięzłych skałach zbiornikowych Polski*. PIG-PIB, Warszawa 2014.
- [11] Suarez A.A.: *The Expansion of Unconventional Production of Natural Gas (Tight Gas, Gas Shale and Coal Bed Methane)*. National Energy Commission, Spain 2012.
- [12] International Monetary Fund. *Box 3.2. Unconventional Natural Gas: a Game Changer?* April 2011.
- [13] Holditch S.A.: *Stimulation of Tight Gas Reservoirs Worldwide*. Paper presented at the Offshore Technology Conference Houston, Texas 2009, OTC-20267-MS.
- [14] Such P., Leśniak G., Słota M.: *Ilościowa charakterystyka porowatości i przepuszczalności utworów czerwonego spągowca potencjalnie zawierających gaz ziemny zamknięty*. Przegląd Geologiczny, vol. 58, nr 4, 2010, pp. 347–351.
- [15] Rybicki C., Blicharski J.: *Problemy przemieszczania się wody złożowej w czasie eksploatacji złóż gazu ziemnego i podziemnych magazynów gazu*. Wiertnictwo, Nafta, Gaz, t. 24, z. 1, 2007, pp. 435–441.



Paweł Zyzański

AGH University of Science and Technology  
ORCID: 0000-0003-0248-7513

## PERFORMANCE ANALYSIS OF A HORIZONTAL WELL LOCATED IN AN UNDERGROUND GAS STORAGE FACILITY

Date of submission:  
28.06.2021

Date of acceptance:  
29.06.2021

Date of publication:  
31.08.2021

© 2021 Author. This is an open access publication, which can be used, distributed, and reproduced in any medium according to the Creative Commons CC-BY 4.0 License

<https://journals.agh.edu.pl/jge>

**Abstract:** Natural gas is the most ecological fossil fuel thanks to lower CO<sub>2</sub> emissions and no dust pollution, hence it is included into raw materials beneficial from the point of view of environmental protection. Natural gas is extracted from deposits often located at great depths by means of both vertical and horizontal drilling, characterised by high efficiency in terms of obtaining the highest possible productivity, which will allow the existing resources of the deposit to be exploited in the shortest possible time.

The paper analyses the influence of factors such as reservoir pressure, the thickness of the reservoir, the length of a horizontal section, average permeability of a reservoir, turbulence coefficient and water exponent on the process of lifting a liquid phase during the operation of a horizontal well located in an underground gas storage facility.

The calculations were carried out using data concerning exploitation of the “B” natural gas field and conducted using the “IHS PERFORM” computer programme, which is the leading industry software for carrying out analyses of productivity changes in gas wells.

In the final part of the article, conclusions are given, summarising the results of the nodal analysis reservoir performance curve (IPR) and well throughput curve (VLP).

**Keywords:** horizontal well, IPR, VLP, gas rate, UGS facility

# 1. Introduction

Energy raw materials, especially environmentally friendly raw materials, are becoming increasingly important and include the natural gas known as “blue fuel”. Natural gas is extracted from deposits often located at great depths by means of both vertical and horizontal drilling.

It is important that both vertical and horizontal wells are characterised by high efficiency in terms of obtaining the highest possible productivity, which will allow the existing resources of the deposit to be exploited in the shortest possible time.

The paper analyses the influence of factors such as reservoir pressure, the thickness of the reservoir, the length of a horizontal section, average permeability of a reservoir, turbulence coefficient and water exponent on the process of lifting a liquid phase during the operation of a horizontal well. The calculations were carried out using data concerning exploitation of the “B” natural gas field and conducted using the “IHS PERFORM” computer programme, which is the leading industry software for carrying out analyses of productivity changes in gas wells. The following correlations were used in the horizontal well performance analysis:

- Joshi’s correlation for calculating productivity for a horizontal well,
- the Hagedorn & Brown correlation for determining the course of pressures in a well for two-phase flow,
- the Lee, Gonzalez & Eakin correlation for calculating changes in gas viscosity,
- the Dranchuk & Purvis – Robinson correlation for calculation of deviation factor of real gas  $z$ .

The results of the calculations are presented in the form of graphs. In the final part of the article, conclusions are given, summarising the results of the analysis. In the further part of the article, the author focused on the course of operation of a horizontal well located in an underground gas storage facility.

## 2. Method section

### 2.1. A brief description of the underground gas storage facility “B”

The Underground Gas Storage Facility (UGS) is located in the partially depleted “B” natural gas field. This field is geologically located in the central part of the pre-Sudetic monocline in the northern edge of Carboniferous tectonic element called the Wolsztyn Dike. The structure of the “B” gas field is formed by a reef in the Zechstein limestone developed on a “paleovoltage” in the Zechstein basement. In the geological section of the reef of the “B” deposit 87.5 m of Zechstein limestone profile was found, developed in the form of permeable and porous rocks. The “B” gas field is massive and stratified with an area of about 1.53 km<sup>2</sup>, with a volumetric energy system [1].

Petrophysical and technological parameters characteristic of the “B” PMG are summarised in Table 1. These parameters were obtained from the B3H well.

**Table 1.** Summary of parameters and data used in the analysis of the effectiveness of operation of the B3H well [2–4]

Parameters for PMG “B” [2]							
Total field resources [million nm <sup>3</sup> ]	Extracted field resources [million nm <sup>3</sup> ]	Buffer gas [million nm <sup>3</sup> ]	Reservoir pressure [MPa]	Reservoir temperature [K]	Average reservoir thickness [m]	Skin effect [-]	Coefficient deviation of gas $z$ [-]
1110	546.367	563.633	18.3	371.15	29	2	0.968
Parameters of reef formations in PMG “B” [2]							
Average effective porosity [%]	Average horizontal permeability of deposit [mD]	Water saturation [%]	Average vertical permeability [mD]	Average clayey [%]	Hydrocarbon content in limestone profile [%]		
14.98	59	14	19	8.14	81.33		
Data of fluids taken for the analysis of efficiency of the B3H well on the “B” PMG [3]							
Water exponent [m <sup>3</sup> /million nm <sup>3</sup> ]	Density of condensate [g/cc]	Density of gas [-]	Density of water [g/cc]	Salinity of water [mg/l]	CO <sub>2</sub> content [%]	Nitrogen content [%]	
5	0.832	0.643	1.07	92.710	0.2298	18.3038	
Casing pipe parameters of horizontal section of B3H well [4]				Parameters of B3H well trajectory [4]			
Drilling depth [m]	Outer diameter [mm]	Inner diameter [mm]	Absolute roughness [mm]	Max. measured depth (MD) [m]	Max. vertical depth (TVD) [m]	Max. borehole angle [°]	
2850	177.8	151.49	0.01651	2850	2489.9	90	

## 2.2. Brief characteristics of the correlations used in the analysis of horizontal well efficiency

The following equation was used to develop a performance curve for a horizontal well Joshi's equation (1) for steady-state flow of a weakly compressible fluid in an anisotropic reservoir, without formation damage [5].

$$q = \frac{2\pi k_H h \Delta p}{B\mu \left\{ \ln \left[ \frac{a + \sqrt{a^2 - \left(\frac{L}{2}\right)^2}}{\frac{L}{2}} \right] + \left(\frac{I_{ani} h}{L}\right) \ln \frac{I_{ani} h}{r_w (I_{ani} + 1)} \right\}} \quad (1)$$

where:

- $q$  – borehole flow rate,
- $\Delta p$  – pressure difference [Pa],
- $B$  – volume factor of gas [–],
- $k_H$  – horizontal permeability [m<sup>2</sup>],
- $h$  – depth of borehole [m],
- $\mu_g$  – gas viscosity [Pa·s],
- $L$  – length of horizontal section of the well [m],
- $r_w$  – radius of the well [m],
- $a$  – half the length of the horizontal well interaction ellipsoid [m],
- $I_{ani}$  – medium anisotropy coefficient [–],
- $k_V$  – vertical permeability [m<sup>2</sup>],
- $r_{eH}$  – radius of the horizontal well interaction range [m].

In Joshi's formula, the function PD(tD) for a horizontal well is proposed, consisting of two members:

- The first describes the horizontal flow and depends mainly on the length of the horizontal section ( $L$ ). The length ( $L$ ) affects the longer half-axis of the ellipsoid ( $a$ ), which is expressed by equation:

$$a = \frac{L}{2} \left\{ 0.5 + \left[ 0.25 + \left( \frac{r_{eH}}{\frac{L}{2}} \right)^4 \right]^{0.5} \right\} \quad (2)$$

- The second term (3) describes the flow in a vertical plane taking into account the medium anisotropy coefficient  $I_{ani}$  expressed by the relation:

$$I_{ani} = \sqrt{\frac{k_H}{k_V}} \quad (3)$$

The natural gas volumetric coefficient  $B_g$  is expressed by the relation:

$$B_g = \frac{V_{p,T}}{V_{sc}} = \frac{P_n T_z z_z}{P_z T_n z_n} \quad (4)$$

where:

- $V_{p,T}$  – the volume occupied by the gas at  $p$ ,  $T$  (in particular under field conditions),
- $V_{sc}$  – volume occupied by gas at standard conditions,
- $B_g$  – volumetric factor of natural gas,
- $P_n$  – pressure at normal conditions,
- $T_z$  – reservoir temperature,
- $z_z$  – deviation factor of real gas under reservoir conditions,
- $P_n$  – reservoir pressure,
- $T_n$  – temperature under normal conditions,
- $z_n$  – deviation coefficient of real gas under normal conditions, assumed to be equal to 1.

Due to the possibility of the occurrence of two-phase flow in a well, the Hagedorn & Brown correlation was used for description, expressing the change of pressure gradients and frictional pressure losses occurring in a pipe in time [6]. This correlation has been derived in the Anglo-Saxon system of units and is not usually converted to the SI system for accuracy of calculations.

In this correlation, the energy conservation equation assuming  $dWs = 0$  is written in the following form:

$$\frac{dp}{dz} = g\rho_{sr} + \frac{2f_f w_m^2}{D} + \rho_{sr} \frac{\Delta \left( \frac{w_m^2}{2} \right)}{\Delta z} \quad (5)$$

The nature of flow in two-phase gas-liquid systems can be determined based on the use of charts, where the flow regime is a function of: flow rate of each phase, fluid properties and the diameter of the extraction pipes. To describe the flow character, dimensionless numbers are used: input fluid  $N_{vl}$  and input gas  $N_{vg}$ , internal diameter  $N_D$  and fluid viscosity  $N_\mu$  defined respectively by the relations [7]:

$$N_{vl} = 1.938 V_{sl} \left( \frac{\rho_L}{\sigma} \right)^{\frac{1}{4}} \quad (6)$$

$$N_{vg} = 1.938 V_{sg} \left( \frac{\rho_L}{\sigma} \right)^{\frac{1}{4}} \quad (7)$$

$$N_D = 1.938 D \left( \frac{\rho_L}{\sigma} \right)^{\frac{1}{2}} \quad (8)$$

$$N = 1.938\mu_L \left( \frac{1}{\mu_L \sigma^3} \right)^{\frac{1}{4}} \quad (9)$$

where (for equations (5), (10) and (11)):

- $f_f$  – flow resistance coefficient,
- $w_m$  – velocity of the mixture of both phases,
- $\rho_{sr}$  – the average density of the flowing fluid expressed by the relation:

$$\rho_{sr} = (1 - \omega_l)\rho_g + \omega_l\rho_l \quad (10)$$

The mixture velocity  $w_m$  is the sum of the surface velocities of the phases:

$$w_m = w_{sc} + w_{sg} \quad (11)$$

In order to calculate the pressure drop in the wellbore from equation (5), the amount of “phase lag” for the fluid  $\omega_l$  and the flow resistance coefficient for the mixture  $f_f$  must be determined in advance. “Phase lag” of the fluid and the average density are determined from the graphs (Figs. 1–3) using the dimensionless numbers  $N_{vl}$  and  $N_{vg}$  previously defined by relations (6)–(9):  $N_D, N_{vl}$ .

“Phase delay” is determined from the graphs in (Figs. 1–3) by the following algorithm [7]:

- calculation of  $N_L$ ,
- determination of the  $CN_L$  from (Fig. 1),
- calculation of the quotient (12):

$$\frac{N_{vl}p^{-1}(CN_L)}{N_{vg}^{0.575}p_a^{-1}N_D} \quad (12)$$

where:

- $p$  – pressure at the well interval for which the pressure gradient is calculated,
- $p_a$  – atmospheric pressure.

Determination of the quotient value based on Figure 2.

Calculation of the auxiliary quotient (13):

$$\frac{N_{vg}N_L^{0.380}}{N_D^{2.14}} \quad (13)$$

Determination of the value of the borehole slope correction  $\Psi$  (Fig. 3).

The magnitude of the “phase lag”  $\omega_l$  is expressed by the formula:

$$\omega_l = \left( \frac{\omega_l}{\Psi} \right) \Psi \quad (14)$$

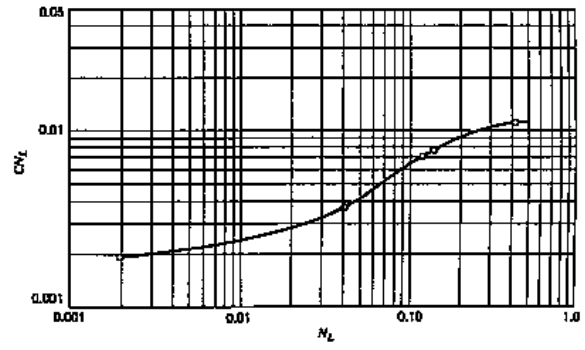


Fig. 1. Plot of  $CN_L$  dependence on  $N_L$  viscosity number [7]

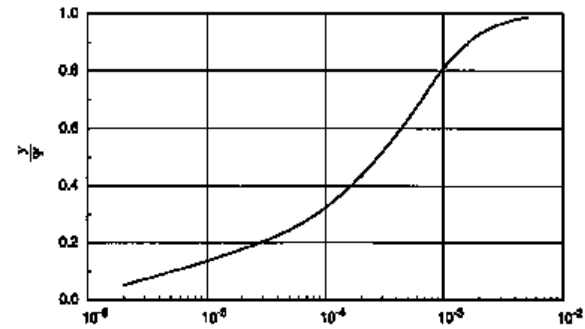


Fig. 2. Diagram of phase delay  $\omega$  as a function of the product

$$\text{of } \frac{N_{vl}p^{-1}(CN_L)}{N_{vg}^{0.575}p_a^{-1}N_D}$$

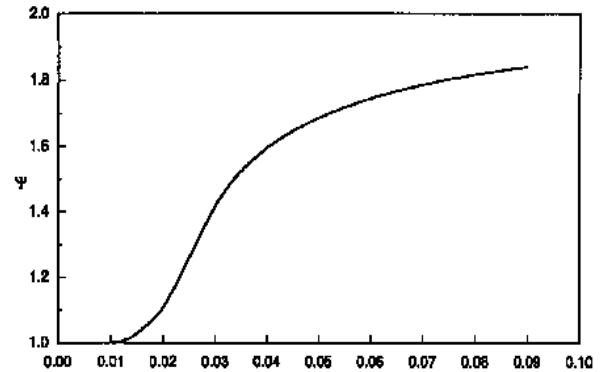


Fig. 3. Correction diagram  $\Psi$  as a function of the product of

$$\frac{N_{vg}N_L^{0.380}}{N_D^{2.14}}$$

The density of the mixture is calculated from equation (13).

The determined density  $\rho_m$  is needed to calculate the hydrostatic pressure and the pressure loss due to friction.

Formula for hydrostatic pressure:

$$\Delta P_{HH} = \frac{\rho_m g \Delta z}{144 \rho_c} \quad (15)$$

The formula for pressure loss due to friction is of the form:

$$\Delta P_f = \frac{\rho_{NS} f V_m D}{\rho_m} \quad (16)$$

where:

- $D$  – pipe inside diameter [ft],
- $f$  – coefficient of friction [-],
- $g$  – gravitational acceleration [32.2 ft/s<sup>2</sup>],
- $\Delta P_{HH}$  – change in pressure [psi],
- $\Delta P_f$  – pressure change due to friction [psi],
- $V_{sl}$  – fluid surface velocity [ft/s],
- $V_{sg}$  – gas surface velocity [ft/s],
- $V_m$  – mixture velocity [ft/s],
- $\Delta z$  – change in height [ft],
- $\mu_L$  – viscosity of the liquid [cP],
- $\rho_L$  – density of liquid [lb/ft<sup>3</sup>],
- $\rho_{NS}$  – density of the fluid in the slip region [lb/ft<sup>3</sup>],
- $\rho_m$  – density of the mixture [lb/ft<sup>3</sup>],
- $\sigma$  – surface tension at the gas/liquid interface [dynes/cm].

Before further use of the correlation, the author checked the ranges of its applicability.

Gas viscosity calculations were performed using the correlation of Lee, Gonzalez and Eakin, expressed by the formula [8]:

$$\mu_g = 10^{-4} K \left[ X \rho_g^Y \right] \quad (17)$$

where:

- $\mu_g$  – gas viscosity [Pa·s],
- $\rho_g$  – density of gas in reservoir at specific pressure and temperature [kg/m<sup>3</sup>].

Parameters  $K$ ,  $X$  and  $Y$  are expressed by relations (18)–(20) [8]:

$$K = \frac{(0.00094 + 0.02 M_{wa}) T^{1.5}}{(209 + 19 M_{wa})} \quad (18)$$

$$X = 3.5 + \frac{986}{T} + 0.01 M_{wa} \quad (19)$$

$$Y = 2.4 - 0.2X \quad (20)$$

where:

- $T$  – temperature of the reservoir [°C],
- $M_{wa}$  – substituted molecular weight of the gaseous mixture.

The dynamic viscosity of water was determined from the Matthews and Russell curve expressed by equation (21) [9]:

$$\mu_w = \left[ \left( \frac{38.3}{T_f^{0.5}} \right) - \left( \frac{14.6}{T_f^{0.25}} \right) + 1.48 \right] \left[ 1 + \left( \frac{C_{ds}}{300} \right) \right] \quad (21)$$

where:

- $\mu_w$  – dynamic viscosity of water [0.001 Pa·s],
- $T_f$  – temperature [°C],
- $C_{ds}$  – concentration of dissolved solids.

The empirical correlation of Dranchuk–Purvis–Robinson (22) expressed by the relation was used to calculate the real gas deviation coefficient  $z$ :

$$q_r = \frac{0.27 p_{pr}}{z T_{pr}} \quad (22)$$

This correlation is valid in the ranges [9]:

$$1.05 < T_{pr} < 3.0 \quad \text{and} \quad 0.2 < P_{pr} < 3.0.$$

The  $q_r$  best value is calculated using the Benedict–Webb–Rubin equation of state.

## 3. Results

### 3.1. Analysis of the effectiveness of the B3H well

In an analysis of the effectiveness of the operation of the B3H well, the author, as mentioned above, took into account the following: the length of the horizontal section, which results from the technology used to drill the well; reservoir pressure; thickness of reservoir; average permeability of the reservoir; turbulence coefficient; and water exponent. These parameters, apart from the first one, are essentially beyond our control, as they are determined by the properties of the discovered reservoir.

Two characteristic curves for the operation of the reservoir and the well are shown in Figure 4. These are: the IPR (Inflow) curve, which represents the inflow of fluid from the reservoir to the well, and the VLP (Outflow) curve, which represents the throughput of the well. These curves intersect at a characteristic point, the abscissa of which, at a well-defined pressure depression, is the flow rate at which the well may be operated. In the case of a need to lift fluids out of the well, it is advisable to define limits to the well's flow rate at which this process occurs without problems. For this reason, two points are determined on the VLP

curve with regard to maximum and minimum flow rates for proper flowing out of the well. In the diagram (Fig. 4), these points are marked as a green square indicating the minimum current flow rate capable of drawing off condensate and a blue triangle indicating the minimum current flow rate for drawing off water. In addition, the minimum current flow rate at which the unfavourable process of bed erosion occurs (bed scouring) is determined. The expenditures for these characteristic points: condensate removal, water removal and sand removal were determined on the basis of calculations carried out with the use of the IHS PERFORM computer program.

If the intersection of IPR and VLP curves is behind the green square, then there are conditions for transportation of condensate, at minimum expenditures and assumed initial factors used in the analysis, amounting for the B3H well to 339,246.4 m<sup>3</sup>/d. On the other hand, in cases where the intersection of the curves is beyond the blue triangle, conditions exist for rising water at minimum flow rate and assumed initial factors used in the analysis, amounting for the B3H well to 478,068.9 m<sup>3</sup>/d. The analysis also shows the flow rate causing erosion of the well with a pink dot. For the B3H well, this value

is 2,662,138.6 m<sup>3</sup>/d, beyond which potential damage to the tubing in the well will occur.

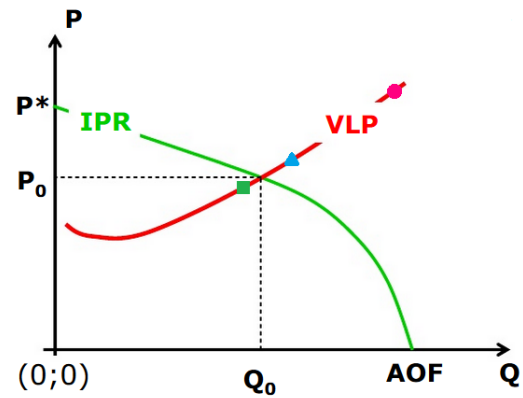


**Fig. 4.** Example of nodal analysis for a well [4], where: IPR – reservoir performance curve, VLP – well throughput curve, P – dynamic bottom pressure, P\* – reservoir pressure, P<sub>0</sub> – bottomhole pressure in the exploited B3H well, Q – flow rate, AOF – maximum potential flow rate, Green square – minimum current flow rate to remove condensate, blue triangle – minimum current flowrate for water removal, pink dot – erosion-inducing flow rate

**Table 2.** Summary of efficiency depending on individual B3H factors

Variant	Length of horizontal section [m]	Gas output [m <sup>3</sup> /d]	Variant	Average field permeability [mD]	Gas output [m <sup>3</sup> /d]
1	440	495,571	1	59	495,426
2	10	301,501	2	1	60,872.9
3	50	442,030	3	50	456,699
4	100	468,077	4	100	638,893
5	200	484,005	5	500	1,318,975
Variant	Reservoir pressure [kPa]	Gas output [m <sup>3</sup> /d]	Variant	Variant turbulence [1/m <sup>3</sup> /d]	Gas output [m <sup>3</sup> /d]
1	18,300	495,423	1	0.070629	495,431
2	16,500	271,320	2	0.035315	684,430
3	17,500	409,426	3	0.105944	408,126
4	19,000	561,896	4	0.141259	355,190
5	20,000	648,156	5	0.194231	304,328
Variant	Reservoir thickness [m]	Gas output [m <sup>3</sup> /d]	Variant	Water exponent [m <sup>3</sup> /million m <sup>3</sup> ]	Gas output [m <sup>3</sup> /d]
1	29	495,010	1	5	495,571
2	10	293,196	2	0.001	495,670
3	20	413,473	3	50	390,285
4	50	641,797	4	100	386,819
5	150	1,051,710	5	150	344,094

### 3.2. Analysis of the efficiency of the B3H well as a function of the length of the horizontal section

Analysis of the graph of pressure vs. gas flow rate as a function of the length of the horizontal section (Fig. 5) shows that a change in this parameter produces significant differences in the results obtained. It is also noticeable that curves 1, 5 have the ability to carry condensate and water, while curves 3, 4 only carry condensate. Whereas curve 2 shows no drift of condensate. It is important that this parameter depends on the drilling, so you can manoeuvre this value in order to obtain the best expenditure. How-

ever, analysing the curve of the gas yield as a function of the length of the horizontal section (Fig. 6) it can be stated that in the range of the length of the horizontal section from 10 to 50 m the curve of the change of the yield from the length of the horizontal section increases significantly, which means that the gas yield also increases significantly. Further on, the curve from the value of the length of the horizontal section from 50 to 440 m flattens, which means that the gas flow rate will increase less and less. What is important here is the fact that after exceeding the above-mentioned value, the greater length of the horizontal section does not translate into an increase in gas output, but only generates greater costs.

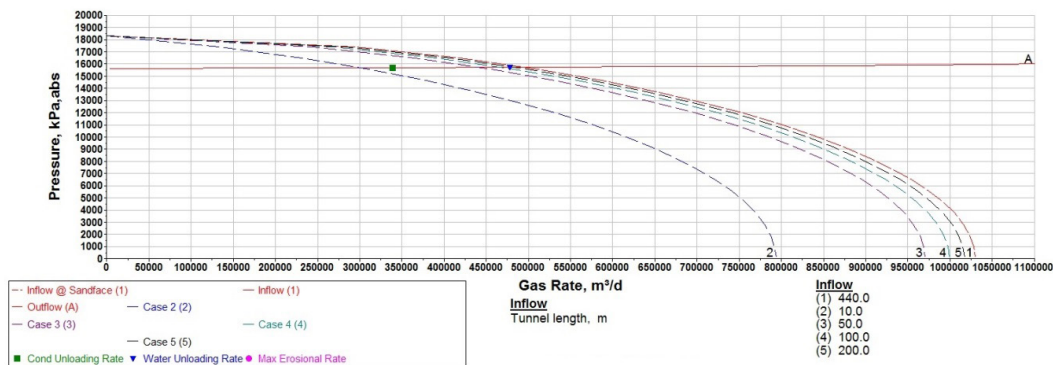


Fig. 5. Graph of pressure vs. gas flow as a function of the length of the horizontal section

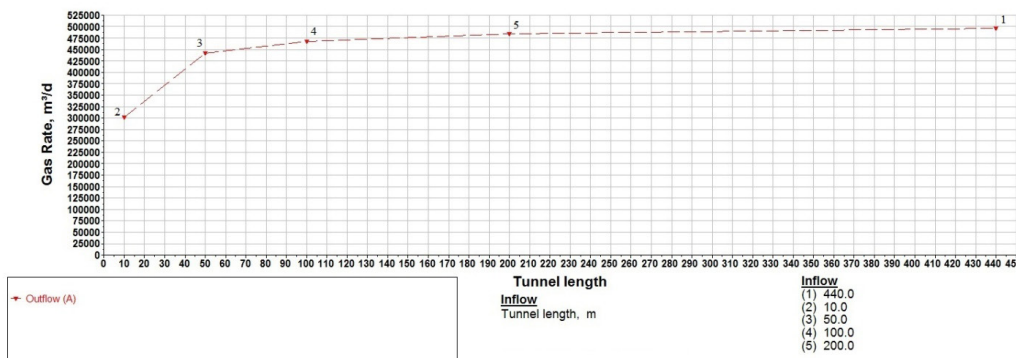


Fig. 6. Graph of gas flow rate vs. the length of the horizontal section

### 3.3. Analysis of the effectiveness of the B3H well in relation to reservoir pressure

By analysing the diagram of pressure vs. gas flow as a function of reservoir pressure (Fig. 7), it may be stated that this parameter is one of the most important ones which influence the effectiveness of well operation. It is also noticeable that for curves 1, 4 and 5, there is a possibility of taking out

condensate and water, while for curve 3 – only condensate. On the other hand, in the case of curve 2, there is no drift of condensate. Analysing the diagram of gas flow in dependence on the pressure in the reservoir (Fig. 8) we can state that in the range of the pressure in the reservoir from 16,500 to 200,000 kPa, the curve of change of the flow in dependence on the pressure in the reservoir increases all the time, which means that the gas flow is also increasing. It is important here that this parameter is crucial in achieving higher gas flow rates in a well.

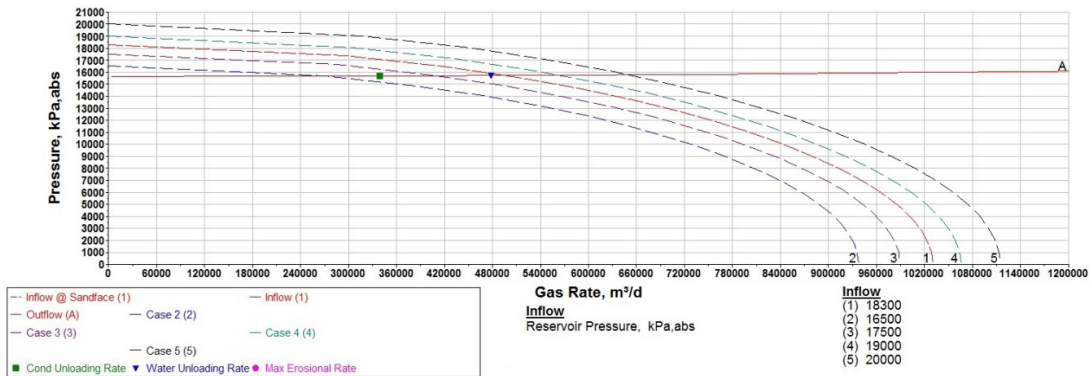


Fig. 7. Graph of pressure vs. gas flow rate as a function of pressure in the reservoir

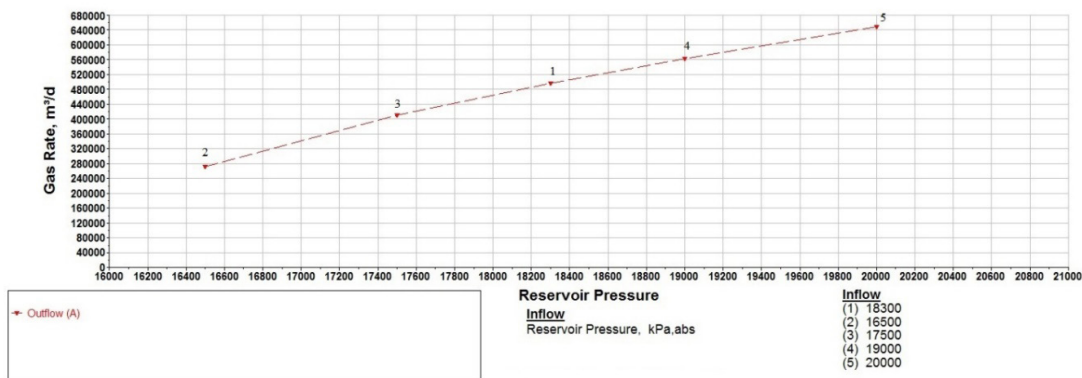


Fig. 8. Graph of gas flow rate vs. pressure in the reservoir

### 3.4. Analysis of effectiveness of the B3H well in relation to the thickness of reservoir

Analysis of the diagram of pressure vs. gas flow rate depending on the thickness of the reservoir (Fig. 9) shows that for curves 1, 4 and 5, there is a possibility of exporting condensate and water, whereas for curve 3 – only condensate. For curve 2, on the other hand, there

is no drift of condensate. Analysing the diagram of gas flow in dependence on the reservoir thickness (Fig. 10) it can be stated that in the range of reservoir thickness from 10 to 150 m the curve of flow change from the reservoir thickness increases, which means that the gas flow also increases. The further course of the curve from the thickness of the reservoir from 50 to 150 m has a greater tendency to increase, which means that the gas flow rate will also increase to a greater extent.

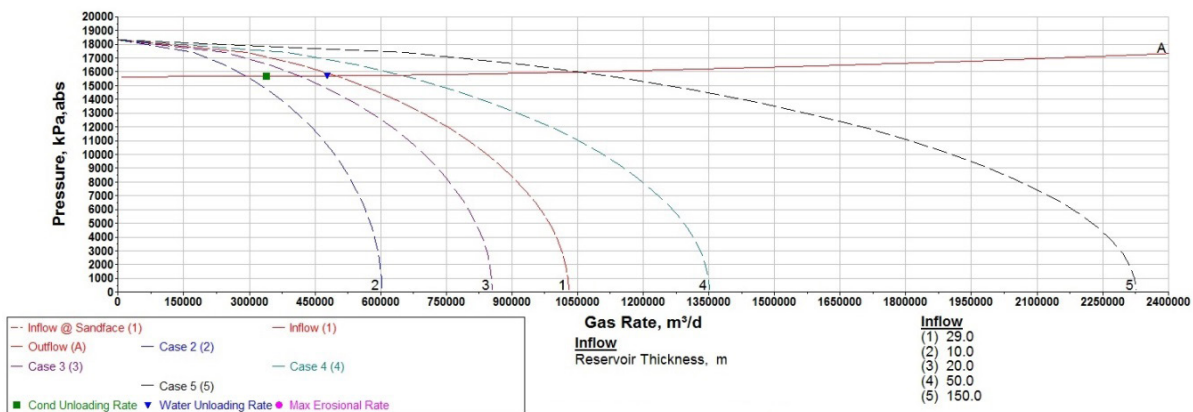


Fig. 9. Graph of pressure vs. gas flow rate as a function of reservoir thickness

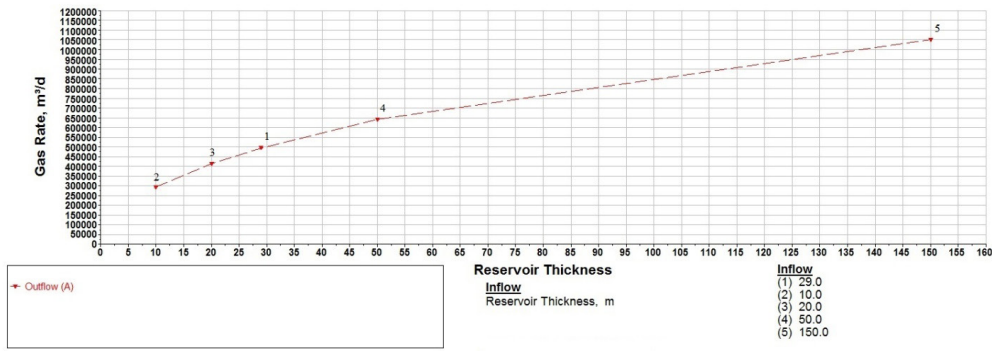


Fig. 10. Graph of gas flow rate vs. thickness of reservoir

### 3.5. Analysis of the effectiveness of the B3H well as a function of the average permeability of the reservoir

Analysing the diagram of pressure vs. gas flow as a function of the deposit average permeability (Fig. 11), it may be stated that in the interval of permeability values from 0 to 60, the values of gas flow increase rapidly, while previously slower. It can also be seen that the IPR (Inflow) curve intersects the VLP (Outflow) curve

behind the blue triangle, so for curves 1 and 4 to 5, it is possible to carry condensate and water out. For curve 3, only condensate outflow is possible.

Analysing the graph of the gas flow rate depending on the deposit average permeability (Fig. 12), it can be stated that in the range of the average permeability values from 1 to 50, the curve of the flow rate change from the permeability ratio increases, which means that the gas flow rate also increases. The further course of the curve from the value of the deposit average permeability from 100 to 500 grows more slowly, which means that the gas flow rate will increase less and less.

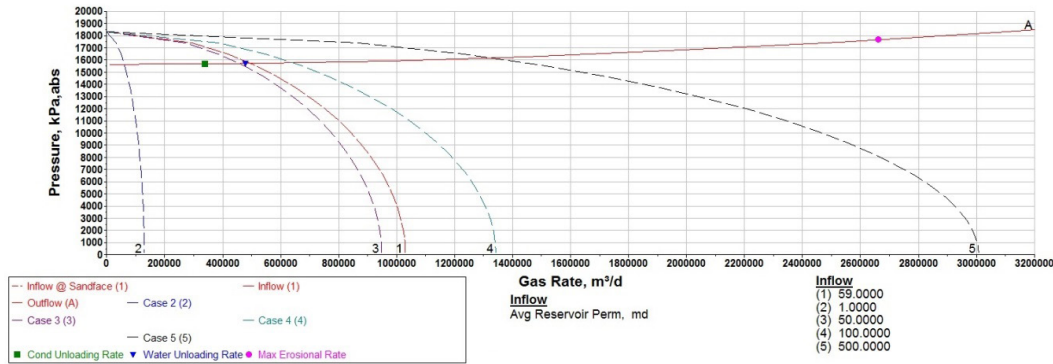


Fig. 11. Graph of pressure vs. gas flow rate as a function of the deposit average permeability

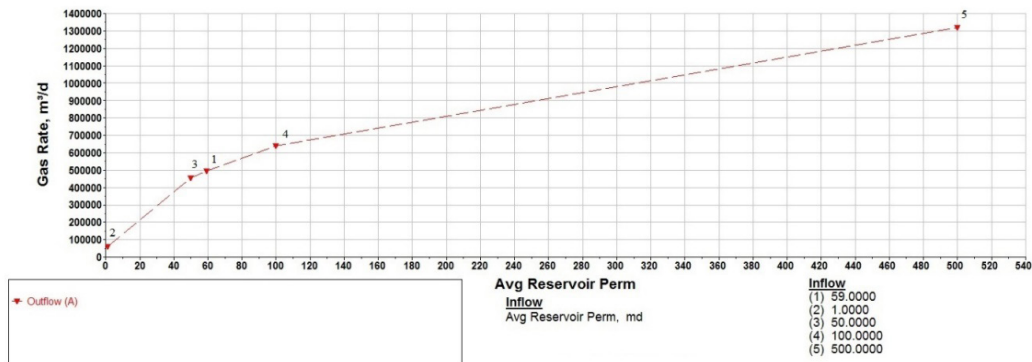


Fig. 12. Graph of pressure vs. gas flow rate as a function of deposit average permeability

### 3.6. Analysis of the efficiency of the B3H well as a function of turbulence ratio

By analysing the diagram of pressure versus gas flow rate as a function of the turbulence ratio (Fig. 13), it can be seen that the higher the turbulence ratio, the lower the gas flow rate. It is also evident that for curves 1 and 2, there is a possibility of removing condensate and water, for curves 3 and 4 – only condensate, whereas for curve 5 there is no possibility of removing both condensate and water. Addi-

tionally, this is the parameter on which the skin effect coefficient depends. Analysing the curve of the gas flow in dependence on the turbulence coefficient (Fig. 14) it can be stated that in the range of the turbulence coefficient value from 0.035315 1/m<sup>3</sup>/d to 0.070629 1/m<sup>3</sup>/d the curve of the flow change from the turbulence coefficient decreases strongly, which means that the gas flow also decreases significantly. The further course of the curve from the value of the turbulence coefficient 0.070629 1/m<sup>3</sup>/d to 0.194231 1/m<sup>3</sup>/d stabilises, which means that the gas flow rate will decrease less and less.

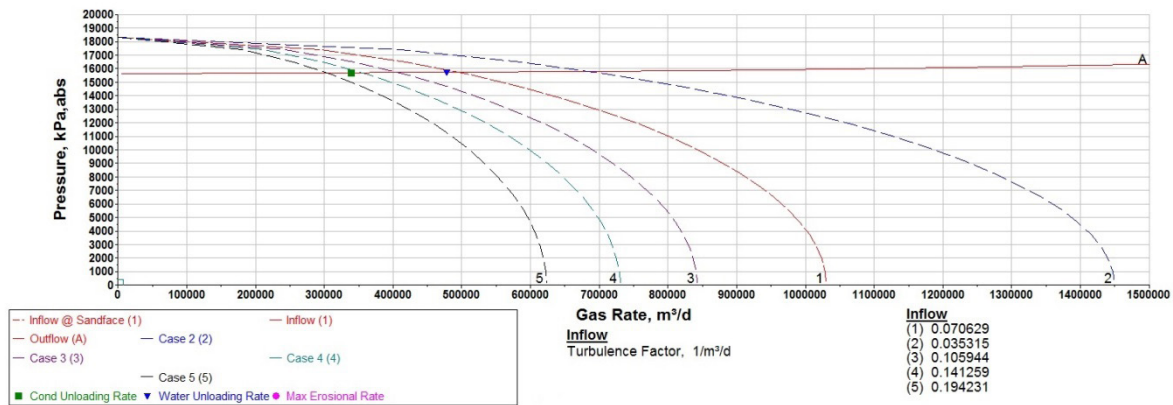


Fig. 13. Graph of pressure versus gas flow as a function of turbulence ratio

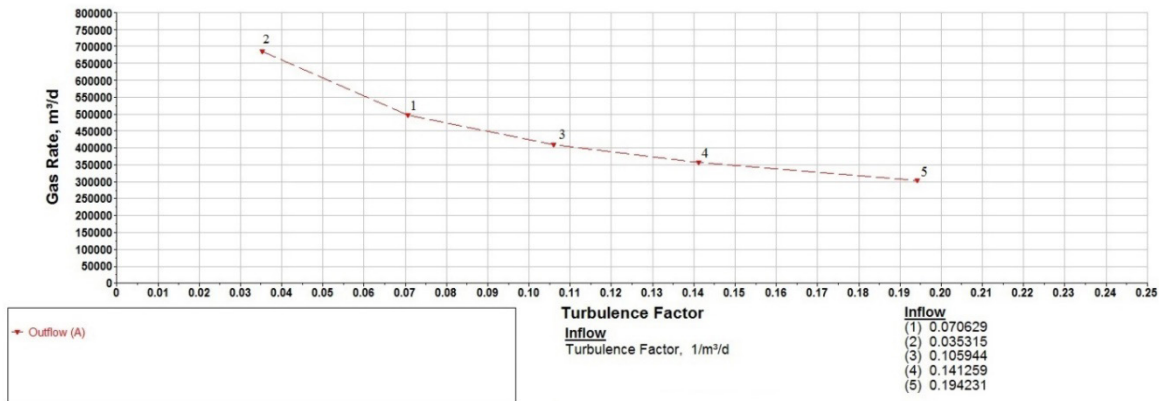


Fig. 14. Graph of gas flow vs. turbulence ratio

### 3.7. Evaluation of the sensitivity of a horizontal well to the water exponent

Analysing the diagram of pressure vs. gas flow rate as a function of the water exponent (Fig. 15), it may be stated that, for specific parameters of the reservoir and the BH3 well, the relations are as follows. Firstly, the higher the water exponent, the lower the gas flow rate.

As regards the pink point on the reservoir productivity curve, it denotes the rate at which liquid and gas would start to destroy the wellbore on the basis of processes such as cavitation; however, since it has a very high value, it is not included in the diagram. The destruction rate decreases as the water exponent increases. It is also noticeable that for curves 3, 4, 5 there is a possibility of removing condensate and water, whereas for curves 1, 2 only condensate can be removed.

Analysing the curve of gas discharge depending on the water exponent (Fig. 16), it can be stated that in the range of the water exponent value  $0.001 \text{ m}^3(\text{l})/10^6\text{m}^3(\text{g})$  to  $5 \text{ m}^3(\text{l})/10^6\text{m}^3(\text{g})$  the curve of change of the discharge from the water exponent decreases slightly, which means that the gas discharge also decreases slightly. The further curve from the value of the water exponent of  $5 \text{ m}^3(\text{l})/10^6\text{m}^3(\text{g})$  to  $50 \text{ m}^3(\text{l})/10^6\text{m}^3(\text{g})$  decreases significantly, which means that the gas flow rate also decreases to a large extent. From the value of the water coefficient of  $50 \text{ m}^3(\text{l})/10^6\text{m}^3(\text{g})$  to  $100 \text{ m}^3(\text{l})/10^6\text{m}^3(\text{g})$ , the curve stabilises, which means practically constant gas emis-

sion. This is due to the fact that the water is initially lifted point-wise upwards, which in the horizontal section merges into a shaft whose water mass is heavy and difficult to lift. Since such a large force is necessary, a greater depression in the reservoir is possible. This increases the output with less risk of water entering the well. Horizontal wells are therefore less sensitive to water inflow into the well. The last section of the curve of the change in flow rate from the water exponent from  $100 \text{ m}^3(\text{l})/10^6\text{m}^3(\text{g})$  to  $150 \text{ m}^3(\text{l})/10^6\text{m}^3(\text{g})$  decreases strongly, which means that the gas flow rate also decreases to a large extent.

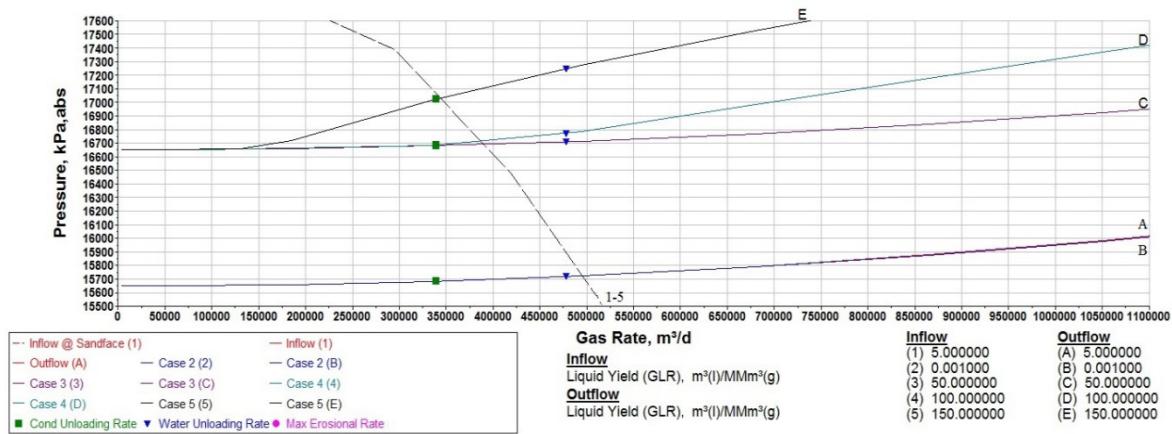


Fig. 15. Plot of pressure versus gas flow versus water exponent

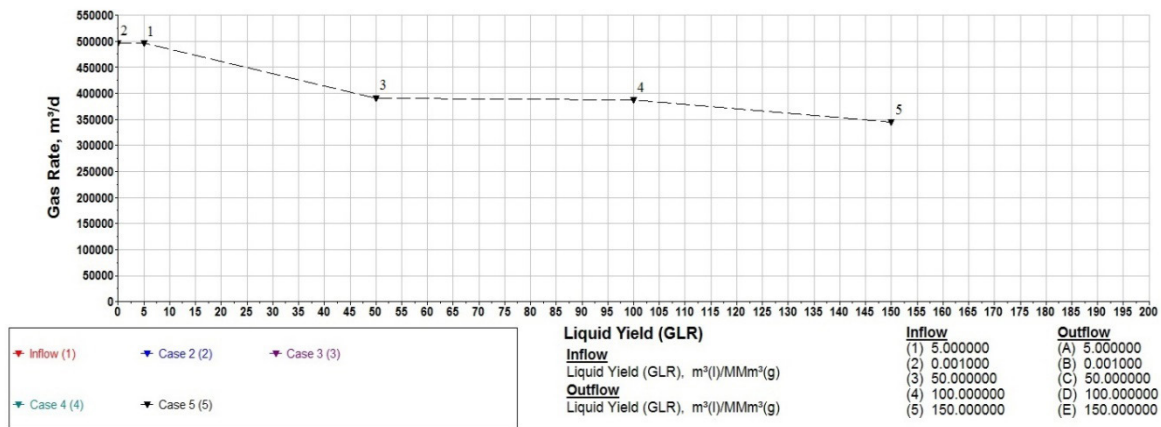


Fig. 16. Plot of pressure vs. gas flow vs. water exponent

## 4. Discussion

1. Horizontal wells are drilled into well-known structures which, after being drilled by vertical wells, provide a great deal of information on the spatial geometry or fracture structure of the reservoir, thus eliminating the risk of a possible unsealing of the reservoir structure through the unintentional drilling of a horizontal well into it.
2. The contact between the horizontal well and the reservoir is determined by the length of the horizontal well, which makes it possible to achieve a higher flow rate at the same depression. Horizontal wells are less sensitive to water inflow into the well because the pressure gradient is distributed over a certain length of the horizontal section.

3. An analysis of the course of the IPR curve (Fig. 5) as a function of the length of the horizontal section shows that the longer the horizontal section, the greater the gas flow rate. A significant increase in the gas discharge can be found in the length range from 10 m to 50 m. For greater values of the length of horizontal sections, the increase in output becomes weaker. It is important here that after exceeding the value of 440 m there is no visible increase in efficiency. It is also noticeable that for lengths of horizontal sections: 440, 200 (curves 1, 5) there is a possibility of carrying away condensate and water (Fig. 6).
4. From the analysis of the IPR curve (Fig. 7) on the pressure in the bed, it can be stated that the higher the pressure in the reservoir, the higher the gas output. A significant increase in gas output can be found in the range of reservoir pressure from 16,500 to 20,000 kPa. It is also noticeable that for the values of pressures in the reservoir: 18,000, 19,000, 20,000 (curves 1, 4, 5) there is a possibility of condensate and water extraction (Fig. 8).
5. From the analysis of the course of the IPR curve (Fig. 9) on the thickness of the deposit it can be stated that the greater the thickness, the greater the gas output. A significant increase of gas yield can be found in the thickness range from 10 m to 150 m. It can also be seen that for thickness values: 29, 50, 150 (curves 1, 4, 5), there is a possibility of condensate and water being carried away (Fig. 10).
6. From the analysis of the IPR curve (Fig. 11) on the average permeability of the deposit, it can be concluded that the higher the average permeability of the deposit, the higher the gas flow rate. A significant increase in the gas output can be found in the range of average reservoir permeability from 1 to 59 mD. For higher values of the vertical permeability of the reservoir, the increase in output increases more strongly. It can also be seen that for values of vertical bed permeability: 59, 100, 500 (curves 1, 4, 5), there is a possibility of condensate and water lift-off (Fig. 12).
7. The analysis of the IPR curve (Fig. 13) on the turbulence ratio shows that the higher the turbulence ratio, the lower the gas flow rate. A significant decrease in gas flow rate can be found in the range of turbulence ratio from 0.035315 1/m<sup>3</sup>/d to 0.070629 1/m<sup>3</sup>/d. For higher values of turbulence coefficients, the decrease in output decreases more strongly. It is also evident that for the values of reservoir vertical permeability: 0.035315; 0.070629 (curves 1, 2), there is a possibility of condensate and water outflow (Fig. 14).
8. From the analysis of the course of the IPR curve (Fig. 15) from the water exponent it can be stated that the greater the water exponent, the smaller the gas output. A significant decrease in the gas yield can be found in the water exponent ranges from 5 m<sup>3</sup>(l)/10<sup>6</sup>m<sup>3</sup>(g) to 50 m<sup>3</sup>(l)/10<sup>6</sup>m<sup>3</sup>(g) and from 100 m<sup>3</sup>(l)/10<sup>6</sup>m<sup>3</sup>(g) to 150 m<sup>3</sup>(l)/10<sup>6</sup>m<sup>3</sup>(g). For values of the water exponent range from 50 m<sup>3</sup>(l)/10<sup>6</sup>m<sup>3</sup>(g) to 100 m<sup>3</sup>(l)/10<sup>6</sup>m<sup>3</sup>(g), the curve stabilises, which means practically constant gas output. This is due to the fact that the water is initially lifted upwards at a point, which in the horizontal section merges into a shaft whose water mass is heavy and difficult to lift. Since such a large force is necessary, a greater depression in the reservoir is possible. This increases the output with less risk of water entering the well. Horizontal wells are therefore less sensitive to water inflow into the well. It can also be seen that for a value of the water exponent of 0.001–5 (curves 2, 1), there is a possibility of condensate and water escaping (Fig. 16).

## 5. Conclusions

In conclusion, it is confirmed that the most important factors having the greatest influence on the efficiency of a horizontal well located in an underground gas storage facility are the following: reservoir pressure, thickness of the reservoir, length of the horizontal section, average permeability of the reservoir, turbulence coefficient and water exponent.

## REFERENCES

- [1] Gąska K., Hoszowski A., Gmiński Z., Kurek A.: *Monografia podziemnych magazynów gazu w Polsce*. Stowarzyszenie Inżynierów i Techników Przemysłu Naftowego i Gazowniczego Oddział Warszawa II, Warszawa 2012.
- [2] Dokumentacja geologiczna złoża gazu ziemnego Bonikowo w kat. B – dodatek nr 1 – PGNiG Oddział Zielona Góra – rozliczenie zasobów, PGNiG SA w Warszawie. Zielona Góra, listopad 2009 [unpublished].
- [3] Dokumentacja wynikowa odwiertu eksploatacyjnego Bonikowo 3H, PGNiG SA w Warszawie. Zielona Góra, kwiecień 2010 [unpublished].

- [4] *Aktualizacja studium-wykonalności dla PMG Bonikowo na bazie częściowo szcerpanego złoża gazu ziemnego Bonikowo*, oprac. Zespół Rzeczoznawców, Grupa Terenowa z Zielonej Góry. Zielona Góra, styczeń 2006.
- [5] Ahmed T.: *Reservoir Engineering Handbook*. Second edition, Gulf Professional Publishing 2007.
- [6] Hagedorn A.R., Brown K.E.: *Experimental Study of Pressure Gradients Occurring During Continuous Two-Phase Flow in Small Diameter Vertical Conduits*. Journal of Petroleum Technology, Vol. 17, April 1965, pp. 475–484.
- [7] *Materiały zebrane podczas praktyki dyplomowej dot. parametrów i zakresu pracy odwiertu horyzontalnego na podziemnym magazynie gazu*. Kraków [unpublished].
- [8] Ahmed T.: *Equation of state and PVT analysis. Applications for Improved Reservoir Modeling*. Second edition, Gulf Professional Publishing 2007.
- [9] Plume R.W.: *Ground-Water Conditions in Las Vegas Valley, Clark County, Nevada. Part 1: Hydrogeologic Framework, Clark County*. Department of Comprehensive Planning 1989.

